Intestinal microbiota programming of alveolar macrophages influences severity of respiratory viral infection

Vu L. Ngo[1#], Carolin M. Lieber[1#], Hae-ji Kang[1], Kaori Sakamoto[2], Michal Kuczma[1], Richard K. Plemper[1&], and Andrew T. Gewirtz[1,3&]

Affiliation:

1. Center for Translational Antiviral Research, Georgia State University Institute for Biomedical Sciences, Atlanta GA 30303, USA.

2. Department of Pathology, University of Georgia College of Veterinary Science, Athens GA 30602, USA

3. Lead contact

# These authors contributed equally to this work

& Denotes co-senior and co-corresponding authors

Correspondence: rplemper@gsu.edu or agewirtz@gsu.edu

Abstract (146 words)

Susceptibility to respiratory virus infections (RVIs) varies widely across individuals. Because the gut microbiome impacts immune function, we investigated the influence of intestinal microbiota composition on RVI and determined that segmented filamentous bacteria (SFB), naturally acquired or exogenously administered, protected mice against influenza virus (IAV) infection. Such protection, which also applied to respiratory syncytial virus and SARS-CoV-2, was independent of interferon and adaptive immunity but required basally resident alveolar macrophages (AM). In SFB-negative mice, AM were quickly depleted as RVI progressed. In contrast, AM from SFB-colonized mice were intrinsically altered to resist IAV-induced depletion and inflammatory signaling. Yet, AM from SFB-colonized mice were not quiescent. Rather, they directly disabled IAV via enhanced complement production and phagocytosis. Accordingly, transfer of SFB-transformed AM into SFB-free hosts recapitulated SFB-mediated protection against IAV. These findings uncover complex interactions that mechanistically link the intestinal microbiota with AM functionality and RVI severity.

One sentence summary: Intestinal segmented filamentous bacteria reprogram alveolar macrophages promoting nonphlogistic defense against respiratory viruses.

41 **INTRODUCTION**

42 Outcomes following exposure to respiratory viruses, such as influenza A viruses (IAV),
43 respiratory syncytial virus (RSV), and severe acute respiratory syndrome coronavirus 2 (SARS-
44 CoV-2), vary widely amongst individuals, ranging from asymptomatic infection to severe lung
45 pathology and/or death. While determinants of such heterogeneity to RVI are likely numerous
46 and complex, we hypothesized that one important factor is gut microbiota composition [1], which
47 is now appreciated to have broad influence over a range of chronic inflammatory diseases and
48 the immune responses with which such diseases are associated [2]. For example, studies comparing
49 mice captured in the wild to those bred for generations in well-controlled vivaria revealed vast
50 differences in their microbiomes that resulted in wild mice having highly and broadly activated
51 immune systems and being relatively resistant to IAV [3,4]. Yet, differences in specific microbial
52 species that can impact RVI outcomes, and how they might do so, have not been well defined.
53 Hence, we studied mice raised in vivaria with discrete defined microbiome differences and,
54 subsequently, mice differing in only the presence or absence of a single common species, namely
55 segmented filamentous bacteria (SFB). We found that gut SFB dictated the phenotype of alveolar
56 macrophages and, consequently, modulated outcomes of RVI.

57 **RESULTS**

58

59 **SFB protects mice from IAV infection**

60 Appreciation of the potential of microbiota to broadly impact health led one commercial
61 rodent supplier to offer "excluded flora (EF)" mice, which were bred in a restricted vivarium that
62 assured absence of a discrete panel of disease-modulating commensal microbes, which might or
63 might not otherwise be present in colonies of "specific pathogen-free (SPF)" mice commonly
64 used in biomedical research [5]. We used such mice as a starting point to probe the influence of
65 microbiota composition on RVI. Specifically, we compared proneness of SPF and EF mice to
66 IAV infection following intranasal administration of 2009 pandemic A/CA/07/2009 (H1N1),
67 herein referred to as CA09, which readily infects mice without need for species adaptation and
68 recapitulates major clinical features of human disease in the animal model [6]. Viral titers in the
69 lung were measured 4 days post-infection (dpi), a time point at which disease symptoms,
70 including mortality, could be assessed although experiments explicitly designed to measure
71 survival were allowed to proceed until 14 dpi, when infectious particles were no longer
72 detectable. Compared to EF mice, SPF mice exhibited significantly reduced lung virus loads.
73 Furthermore, SPF mice did not show hypothermia and weight loss observed in EF mice **(Figure**
74 **1A)**. Additionally, some mice of the EF mice required euthanasia. These results suggested that
75 one or more of the microbes specifically excluded from EF mice might confer protection against
76 IAV.

77 Of the panel of organisms known to be absent in EF mice, segmented filamentous
78 bacteria (SFB) stood out as a potential modulator of IAV proneness in that SFB, despite being a
79 strict anaerobe and, thus, restricted to the intestinal luminal surface, is known to systemically

80 impact T-lymphocytes [7,8]. Furthermore, SFB is a major contributor to, albeit not the sole
81 mediator of, spontaneous resistance of mice to rotavirus (RV), an intestinal pathogen, that arose
82 in some mouse colonies [9]. SFB is very challenging to culture but can be isolated, maintained, and
83 studied by administering it via fecal microbial transplantation (FMT). Hence, mice lacking SFB
84 but otherwise carrying a complex SPF microbiota, herein referred to as SFB^- mice, were
85 administered a FMT from other SFB^- mice, mice containing SFB as one natural component of
86 their SPF microbiota, or germ-free mice that had been monoassociated (MA) with SFB. Such
87 mice were inoculated with CA09 one-week post-FMT and euthanized 4d later to measure lung
88 viral titers or monitored for 14 days to assess survival. Mice receiving FMT from donors
89 naturally colonized with SFB exhibited IAV titer reductions of approximately one order of
90 magnitude compared to animals that lacked SFB and, concomitantly, clinical signs of IAV
91 infection were ameliorated **(Figure 1B).** FMT from SFB-MA mice fully recapitulated such
92 protection while administering feces from germ-free mice was without effect (**Figure S1A).**
93 Thus, administering SFB^- mice a FMT from SFB-MA mice, hereafter referred to as
94 administering SFB, recapitulated the differential proneness of EF and SPF mice to IAV
95 infection, thus providing a tractable model to investigate how the presence of this specific gut
96 microbiota constituent, within a complex microbial ecosystem, reduced IAV infection in the
97 lung.

98 SFB-mediated protection against IAV infection was evident, albeit seemingly not
99 maximal, two days post SFB administration and was undiminished three months later (longest
100 time tested) despite gut SFB levels having declined by over 60-fold from peak to a stable plateau
101 by this time **(Figure 1C and Figure S1B).** In accord with its relative abundance not being a
102 critical variable, SFB colonized 24-week-old mice at 10-fold lower levels than 5-week-old mice

103 but still protected them against IAV infection **(Figure S1C)**. Consistent with previous
104 observations that SFB only resides in the gut lumen or attached to the apical epithelial gut
105 surface [10], SFB was readily detected by PCR in the ileum, but was not found in the lung or
106 spleen **(Figure 1D)**. Histopathologic examination of lung tissue did not detect any impact of SFB
107 itself on the lung but revealed a striking suppression of IAV-induced lung pathology **(Figure**
108 **1E)**. Such protection of lung tissue was potentially attributable to the 1-log reduction in viral
109 titers conferred by SFB colonization but also hinted at the possibility that SFB had reduced IAV-
110 induced inflammatory signaling.
111

112 **SFB-mediated protection against IAV is not explained by known candidate mechanisms**

113 SFB-mediated lasting protection against IAV contrasted with its transient protection
114 against RV [9], suggesting that the former might be mediated by adaptive immunity. However,
115 SFB-mediated protection against IAV was fully maintained in *Rag1*$^{-/-}$ mice, which lack most T
116 and B lymphocytes, arguing against this notion **(Figure 2A)**. Innate antiviral immunity typically
117 involves interferon and can involve innate lymphoid cells (ILC) and/or IL-22 and IL-17. Yet,
118 SFB-mediated protection against IAV was also maintained in *Ifnar*$^{-/-}$ mice, which lack type I
119 interferon signaling, *Rag1*$^{-/-}$-*Il2rg*$^{-/-}$, which lack type 3 ILC, and upon antibody-mediated
120 neutralization of IL-17 and IL-22 **(Figure 2B-D)**. SFB-mediated protection against IAV was
121 furthermore maintained in *Stat1*$^{-/-}$ animals, which are broadly compromised in IFN signaling
122 **(Figure 2E)**. These results argue against a role for any of these candidate host mechanisms in
123 mediating SFB's protection against IAV infection. We also considered a candidate microbial
124 mechanism. Specifically, we hypothesized that the protection against IAV conferred by SFB
125 might reflect that it induced an array of complex changes in other taxa that might then broadly

126 impact innate immunity. However, SFB's protection was maintained in Altered Schaedler flora
127 (ASF) mice, which harbor only a minimal 8-species microbial community [11], thus arguing
128 against this possibility.
129
130 **SFB-mediated protection against IAV, RSV and SARS-CoV-2 is associated with**
131 **preservation of resident lung phagocytes**
132 That candidate mechanisms were not experimentally substantiated led us to utilize less
133 targeted approaches to investigate how SFB gut colonization protected mice against IAV. First,
134 we performed transcriptomic profiling of whole lungs harvested from mice that were untreated
135 (naïve) or administered SFB, CA09, or a combination thereof. The results of this RNA-seq
136 analysis were presented as a heat map, showing 4-5 individual mice per condition, of all genes
137 whose expression was significantly altered in response to any of the three treatments **(Figure**
138 **3A)**. It illustrated that SFB, by itself, had almost no impact on lung gene expression, whereas, as
139 expected, IAV infection, by itself, markedly remodeled the lung transcriptome. Strikingly, such
140 IAV-induced changes in gene expression were absent in SFB-colonized mice, indicating that the
141 presence of SFB in the gut broadly ameliorated IAV's impact on lung tissue. The majority of
142 genes induced by CA09 were related to immunity and inflammation and thus accorded with the
143 view that much of the lung pathology in IAV infection is driven by the immune system [12] and,
144 furthermore, the notion that SFB had dampened such responses.
145 We next used flow cytometry to examine the impact of SFB and IAV on lung populations
146 of immune cells, focusing on innate cells given that our results from *Rag1*$^{-/-}$ mice had suggested
147 lymphocytes were not required for SFB-mediated protection against IAV. Consistent with other
148 studies, intranasal administration of CA09, by itself, induced a stark depletion of basally-resident

149 CD103^{+} dendritic cells (cDC1) and alveolar macrophages (AM), which was followed by
150 increased abundance of a panel of inflammatory cells including neutrophils, monocytes, and
151 natural killer cells [13]. SFB, by itself, had only modest impacts on levels of lung leukocytes,
152 slightly increasing abundance of AM, but wholly prevented the changes induced by CA09
153 **(Figure 3B and Figure S2)**. Preventing these CA09-induced changes in lung cellularity and
154 disease was not SFB strain-specific as similar protective effects resulted from colonization of the
155 gut by SFB strains isolated in 3 different continents **(Figure S3)**. Nor were SFB impacts specific
156 to IAV. Rather, SFB colonization also reduced viral loads and prevented changes in lung
157 cellularity, and reduced pro-inflammatory gene expression, following inoculation of mice with
158 respiratory syncytial virus (RSV) and mouse-adapted SARS-CoV-2 **(Figure S4)**, which,
159 irrespective of SFB, did not cause clinical signs of disease.

160 To investigate the extent to which SFB-mediated prevention of IAV-induced changes in
161 lung cellularity simply reflected lower IAV loads, we pharmacologically restricted IAV
162 replication via 4'-fluorouridine (4'-FIU), a broad-spectrum nucleoside analog inhibitor that we
163 recently reported reduces viral titers and disease symptoms up to 60 hours following
164 administration of IAV, RSV, and SARS-CoV-2 [14,15]. SFB^{-} mice received 4'-FIU via oral gavage
165 at different dose levels in a once daily (q.d.) regimen beginning 24 hours post-inoculation. At
166 this time, IAV levels and immune cell populations were similar in SFB^{-} and SFB-administered
167 mice **(Figure S2C)**, which we hereafter refer to as SFB^{+} mice. As expected, administration of 4'-
168 FIU to SFB^{-} mice dose-dependently suppressed IAV replication to a similar or greater extent
169 than SFB **(Figure 3C)**. Like SFB, 4'-FIU administration prevented the CA09-induced
170 appearance of inflammatory cells in the lung. However, even the highest dose of 4'-FIU, which
171 lowered IAV titers by over three orders of magnitude and markedly reduced inflammatory cell

172 recruitment, did not mitigate CA09-induced ablation of cDC1 or AM. This result suggested that
173 the persistence of AM and cDC1 in SFB$^+$ mice was not entirely a consequence of reduced viral
174 loads and/or inflammation but rather implied that maintenance of these cells may contribute to
175 suppression of IAV.
176

177 **Alveolar Macrophages are required for SFB-mediated protection against IAV**

178 Potential roles for cDC1 and AM in SFB-mediated protection against IAV were tested in
179 mice harboring deficiencies in these cells. We observed that SFB-mediated protection against
180 IAV was maintained in *Batf3*$^{-/-}$ mice, which wholly lack cDC1 [16], but was greatly reduced in
181 *Csf2*$^{-/-}$ mice, which have a 70% reduction in basal AM levels [17] **(Figure 4 A&B)**. The role of
182 AM was further examined by depleting these cells with clodronate liposomes [18], which we
183 verified efficiently removed AM but did not alter levels of other lung innate immune cells
184 **(Figure 4Ci)**. Depletion of AM, by itself, did not significantly impact IAV titers or clinical signs
185 of disease but eliminated the ability of SFB to lower lung IAV load, ameliorate hypothermia and
186 weight loss, and prevent death **(Figure 4Cii)**. These results suggested that SFB-mediated impacts
187 on AM were germane to its protection against RVI. SFB-mediated maintenance of AM levels
188 could conceivably have reflected increased generation of these cells, which can occur from
189 monocyte progenitors migrating to the lung or local self-renewal [19], or that SFB colonization had
190 resulted in AM resisting death upon RVI. SFB's prevention of AM depletion following CA09
191 inoculation associated with prevention of IAV-induced caspase-3 activation **(Figure 4D)**, which
192 marks AM commitment to cell death [20], and increased expression of CD71 **(Figure 4E)**, which
193 associates with enhanced phagocytosis and survival [21,22]. Furthermore, SFB colonization
194 increased AM expression of proliferation marker Ki-67 **(Figure 4F)**. Collectively, these results

195 suggested that SFB colonization may have increased AM self-renewal and, furthermore,
196 "emboldened" AM to resist IAV-induced depletion, resulting in maintenance of a robust AM
197 population following IAV infection.
198
199 **SFB's preservation of AM enables their sustained protection of EC from IAV infection**
200 Airway epithelial cells (AEC) are primary replication sites of respiratory viruses,
201 including IAV, RSV, and SARS-CoV-2. Specifically, in the case of highly pathogenic H1N1
202 IAV, ciliated AEC are the predominant host for virus replication and generation of progeny
203 virions [23]. AM are known to protect lung AEC from IAV infection, particularly at early time
204 points following IAV-infection, i.e. prior to their depletion [24]. Thus, we predicted that SFB's
205 preservation of AM following CA09 inoculation might result in lower viral loads in AEC in
206 SFB^+ mice. Indeed, the percentage of lung AEC, type I and II, as well as conducting AECs,
207 displaying detectable levels of a recombinant CA09 that encodes GFP, by flow cytometry, was
208 significantly reduced in SFB^+ mice 4 days post-inoculation **(Figure 4G and Figure S5)**.
209 Depletion of AM by clodronate liposomes in SFB^+ mice increased IAV levels to that of SFB^-
210 mice in all three lung AEC types. These results indicate that SFB-induced AM persistence
211 following IAV infection enables sustained AM-mediated protection of EC, likely contributing to
212 lower IAV burden and ameliorated pathology.
213
214 **Persistence of SFB^+ AM upon RVI is cell-intrinsic**
215 Persistence of AM in CA09-infected SFB^+ mice was potentially attributable to SFB
216 altering the lung environment and/or reflect that AM themselves had been intrinsically
217 transformed to better withstand IAV challenge. To differentiate between these possibilities, we

218 adoptively transferred FACS-sorted AM from SFB^+ and SFB^- mice to SFB^- mice using donor
219 mice with a CD45.1 subtype, thereby enabling distinction of endogenous and transplanted cells
220 **(Figure 5A)**. The degree to which AM harvested from SFB^+ and SFB^- mice, hereafter referred to
221 as SFB^+ and SFB^- AM, engrafted following transplant was similar, comprising about 15% of the
222 total AM in their new host. CA09 infection did not significantly alter proportions of endogenous
223 vs engrafted AM in recipients of SFB^- AM but led to SFB^+ AM (i.e. engrafted) becoming their
224 host's majority AM population. This shift in AM proportions reflected that endogenous AM in
225 both recipient groups as well as engrafted SFB^- AM were all depleted by CA09 infection,
226 whereas engrafted SFB^+ AM fully resisted CA09-induced depletion and, concomitantly, lacked
227 Caspse-3 activation, despite having been transplanted into an SFB-free host. Thus, colonization
228 of the gut with SFB intrinsically altered AM to withstand IAV-induced depletion.
229 The ability of transplanted SFB^+ AM to withstand IAV-induced depletion could
230 potentially have reflected that, in the donor mice, SFB colonization had phenotypically
231 transformed resident AM and/or led to these cells being replaced by newly recruited monocytic
232 precursors, which then became AM. That SFB^+ mice did not exhibit a basal or IAV-induced
233 elevation of monocytes chemo-attractants or monocyte-derived AM, both of which were readily
234 evident in IAV-infected SFB^- mice, argued against the "AM replacement" mechanism **(Figure
235 5B)**. Furthermore, administering SFB to mice after AM transplant led to similar persistence of
236 both CD45.2 (endogenous) and CD45.1 (exogenous) cells following IAV infection **(Figure 5C)**,
237 thus strongly indicating that SFB colonization changed the phenotype of lung resident AM.
238
239 **SFB^+ AM exhibited inflammatory anergy and enhanced C1qa-mediated antiviral function**

240 Differences between SFB^+ and SFB^- AM were characterized *ex vivo* as schematized
241 **(Figure 6A).** Profiling of basal gene expression (i.e. without IAV exposure) by RNA-seq found
242 that only 24 of the 15,510 genes expressed by AM were differentially expressed between SFB^-
243 and SFB^+ AM **(Figure 6B)**, 18 of which were both confirmed by PCR and biologically
244 replicated in a distinct mouse cohort **(Figure S6A).** Six of the genes upregulated in SFB^+ AM are
245 associated with an M2 macrophage phenotype. Yet, quantitation of surface expression markers
246 previously used to distinguish M1 vs M2 phenotypes [25] did not reveal differences between SFB^+
247 and SFB^- AM **(Figure S6B)**. The genes most prominently up- and down-regulated, respectively,
248 in SFB^+ AM were Tsc22d3 and Notch-4, which, respectively, function in suppressing and
249 activating pro-inflammatory gene expression [26,27], suggesting such signaling might be dampened
250 in SFB^+ AM. Indeed, we found that SFB^+ AM lacked the robust UV-irradiated IAV-induced
251 activation of pro-inflammatory gene expression exhibited by SFB^- AM **(Figure 6C and Figure**
252 **S7C)**. Such inflammatory anergy was partially recapitulated by antibody-mediated neutralization
253 of Notch-4 suggesting that the SFB-induced reduction in AM Notch-4 expression in SFB^+ AM
254 contributed to this *ex vivo* phenotype and, moreover, the reduced inflammation observed in IAV-
255 infected SFB^+ mice. As noted above, in SFB^- mice, IAV infection resulted in depletion of AM,
256 which are then replaced by newly recruited monocytes, some of which will acquire AM cell
257 surface markers. Such "replacement AM" lacked any hint of inflammatory anergy. Rather, they
258 exhibited robust inflammatory responses to IAV, similar to those of the AM they replaced
259 (Figure S6H).
260 The small panel of genes upregulated in SFB^+ AM also included some known to function
261 in antiviral resistance, including complement C1qa and Ifitm1, thus suggesting that SFB^+ AM
262 were not anergic to IAV per se but, rather, might have better virus neutralizing capacity. We

263 examined this possibility by incubating CA09 stocks with AM for 45 min at which time AM
264 were removed by centrifugation and supernatant infectious titers and IAV genomes quantified.
265 SFB^- AM lowered the infectious titers of the CA09 stocks to which they were exposed, at 37ºC
266 but not 4ºC, but the extent of reduction was 150-fold greater for SFB^+ AM (**Figure 6Di**). This
267 greater reduction in titer was accompanied by only 5-fold lower levels of PCR-quantifiable IAV
268 genomes in supernatants of SFB^+ AM (**Figure 6Dii**). This led us to hypothesize enhanced
269 neutralization of IAV by complement and/or other products secreted by SFB^+ AM. Indeed, we
270 found that, even when SFB^+ AM were not exposed to virus, their supernatants from 18h cultures
271 had greater capacity than those from SFB^- AM to lower CA09 infectious titers **(Figure 6Diii**).
272 Such enhanced ability of SFB^+ AM supernatants to lower IAV titers was fully reversed by
273 antibody-mediated removal of C1qa and, moreover, was not observed in $C1qa^{-/-}$ SFB^+ AM
274 **(Figure S6C)**. These results accord with recent observations that C1qa can directly bind IAV
275 and reduce its infectivity [28]. In contrast to AM themselves, which when incubated with CA09
276 stocks lowered both levels of infectious virus (i.e. titer) and levels of viral RNA, AM
277 supernatants did not impact levels of viral RNA (**Figure S6E**) suggesting the enhanced antiviral
278 capacity of SFB^+ AM might also involve increased viral absorption and/or uptake, possibly as a
279 result of viral particles being more decorated with C1qa [29]. In accord with this notion, reductions
280 in IAV genomes in supernatants of AM/CA09 mixtures were paralleled by increased IAV
281 genomes in AM lysates **(Figure 6Div**). The relative increase in IAV genomes in SFB^+, compared
282 to SFB^-, AM lysates was maintained amidst chlorpromazine, but not latrunculin treatment,
283 neither of which impacted cell viability, suggesting it might reflect enhanced phagocytosis
284 uptake by SFB^+ AM (**Figure S6G**). In contrast to our hypothesis, increased uptake of CA09 was
285 evident in $C1qa^{-/-}$ SFB^+ AM (Figure S6D) suggesting SFB^+ AM may be more phagocytic in

286 general. In accord with this notion, SFB^{+} AM exhibited modestly greater uptake of IgG-coated
287 fluorescent beads *ex vivo* and bioparticles *in vivo* **(Figure S6F**). Exploring the fate of CA09
288 internalized by AM during the 45 min exposure period found that, 24 h following media
289 replacement, AM supernatants had few infectious virions while lysates contained few detectable
290 IAV genomes **(Figure 6Div**) thus suggesting that AM were not permissive for CA09 replication,
291 but rather constituted a dead end for the virus. Collectively, these results indicate that elevated
292 C1qa expression and enhanced phagocytosis drove the increased antiviral capacity of SFB^{+} AM.
293 Measure of C1qa protein by ELISA confirmed that SFB colonization increased
294 expression of C1qa in AM isolated from whole lung and bronchoalveolar lavage fluid (BALF)
295 and, moreover in whole BALF **(Figure 6E)**. Furthermore, experiments in *C1qa*$^{-/-}$ mice indicated
296 that C1qa played a central role in SFB's suppression of IAV in vivo. Specifically, in *C1qa*$^{-/-}$
297 mice, SFB colonization did not lower viral titers or protect lung epithelial cells from IAV
298 infection following CA09 inoculation (Figure 6F). Concomitantly, SFB's ability to ameliorate
299 disease symptoms, including weight loss and hypothermia was markedly reduced in *C1qa*$^{-/-}$ mice
300 relative to *C1qa*$^{+/+}$ mice. Nonetheless, colonization of *C1qa*$^{-/-}$ mice with SFB still conferred
301 modest but statistically significant reductions in weight loss and mortality. Moreover, SFB
302 colonization of *C1qa*$^{-/-}$ suppressed CA09-induced pro-inflammatory gene expression, gross lung
303 pathology, and infiltration of inflammatory cells into the lungs. The reduced but not eliminated
304 ability of SFB to suppress symptoms of IAV infection in *C1qa*$^{-/-}$ mice associated with SFB
305 colonization partially protecting AM against IAV-induced depletion. Thus, C1qa was germane to
306 SFB's ability to impede IAV infection and its consequences but nonetheless SFB ameliorated
307 IAV-induced lung inflammation irrespective of C1qa and viral titer.
308

309 **SFB-induced reprogramming of AM protects mice against IAV infection**

310 The starkly different transcriptional responses of SFB$^-$ and SFB$^+$ AM led us to investigate
311 the general metabolic states of these cells via Seahorse analysis. The basal metabolic states of
312 SFB$^-$ and SFB$^+$ AM differed only modestly with SFB$^+$ AM exhibiting a small reduction in
313 glycolysis (Figure S7A). In contrast, inoculating SFB$^-$ mice with CA09 led to stark increases in
314 AM ATP production and glycolysis, which were wholly absent in SFB$^+$ mice thus paralleling
315 above-described changes in inflammatory parameters in UV-IAV induced changes in AM
316 proinflammatory gene expression observed *ex vivo*. Lastly, we examined the extent to which
317 SFB-induced reprogramming of AM contributed to SFB's protection against IAV infection.
318 Specifically, we performed an additional series of AM transplant experiments designed to
319 measure impacts on IAV levels and clinical-type parameters. Consistent with the notion that
320 AM, prior to their depletion, protect against IAV infection [24], we observed that administration of
321 SFB$^-$ AM to a host replete with endogenous AM resulted in a modest reduction in IAV titers,
322 gross lung damage, hypothermia, weight loss, and death following CA09 inoculation **(Figure**
323 **7A)**. Administration of SFB$^+$ AM provided markedly greater protection against this IAV
324 challenge, approximating the level conferred by administration of SFB itself, as assessed by all
325 parameters measured. Analogous patterns of results were seen following transfer of SFB$^+$ and
326 SFB$^-$ AM into mice deficient in endogenous AM, achieved via use of *Csf2*$^{-/-}$ mice or chlodronate
327 administration **(Figure 7B and 7C)**. Analogous to results obtained in *C1qa*$^{-/-}$ mice, transplant of
328 C1qa$^{-/-}$ SFB$^+$ AM into SFB$^-$ mice did not reduce viral titers or protect lung cells from IAV
329 infection following CA09 inoculation but nonetheless reduced indices of inflammation and
330 conferred a modest clinical-type benefit **(Figure S7B)**. *Ex vivo* blockade of Notch-4 on SFB$^-$ AM
331 prior to transplanting them also enhanced their ability to withstand IAV-induced depletion,

332 protect EC from IAV infection, and ameliorate CA09-induced disease, but did not impact level
333 of viral genomes in the lung **(Figure S7C)**, suggesting the ability of transplanted SFB^+ AM to do
334 so was not mediated solely by dampened inflammatory signaling but also required such AM
335 have enhanced antiviral function. Thus, SFB colonization of the gut stably and broadly altered
336 the AM phenotype enabling these cells to better protect their hosts from lethal RVI.

337 **DISCUSSION**

338 Positioned in the lung lumen to enable their guarding the surfaces of O_2 and CO_2
339 exchange, AM are amongst the first cells to encounter inhaled threats including respiratory
340 viruses. We show herein that how AM respond to respiratory viruses is dramatically altered by
341 the composition of the intestinal microbiota. Specifically, we report that colonization of the
342 intestine by SFB, naturally acquired, or exogenously administered, markedly attenuates IAV-
343 induced AM pro-inflammatory gene expression while increasing ability of AM to disable IAV.
344 This seemingly paradoxical phenotypic differences between SFB^- and SFB^+ AM is reminiscent
345 of the comparison of blood monocytes and intestinal macrophages wherein the latter are more
346 phagocytic but yet exhibit inflammatory anergy [30]. An important aspect of SFB-induced
347 reprogramming of AM is that it resulted in resistance of RVI-induced depletion and thus
348 sustained protection of lung epithelial cells. Collectively, the consequences of SFB-induced AM
349 reprogramming resulted in lower viral titers, reduced inflammation, and reduced disease severity.

350 While the general concept that microbiota composition in total can influence immune
351 phenotype and, proneness to infection is established [31,32], we were surprised that the presence of
352 a single common commensal bacterial species, amidst the thousands of different microbial
353 species that variably inhabit the mouse gut, had such strong impacts in RVI models and,
354 furthermore, that such impacts were largely attributable to reprogramming of AM. The extent to
355 which SFB is present in humans is not well defined but it has been reported to be frequently
356 present in children in some regions [33] and was unequivocally shown to be present in some adult
357 individuals [34]. Independent of a specific role for SFB, however, our findings speak strongly to
358 the potential of gut microbiota to influence proneness to RVI, especially via programming of
359 AM. Both AM pro-inflammatory gene expression and AM depletion are known to correlate with

360 RVI severity in humans but determinants of inter-individual heterogeneity in AM responses have
361 not been defined [33]. We consider it highly unlikely that SFB is the only gut microbe capable of
362 impacting AM phenotype and, consequently, proneness to RVI. Rather, we posit that AM are a
363 key component of the gut-lung axis wherein an individual's microbiota in its entirety is a
364 determinant of disease outcome following exposure to an array of respiratory viruses.

365 The observation that SFB^+ AM maintained an IAV-resistant phenotype following
366 transplant to SFB^- mice is consistent with observations that AM have stable cell-type specific
367 patterns of gene expression and methylation even when cultured extensively *ex vivo* [35].
368 Moreover, it accords with recently increasing appreciation that AM can be "trained" to display
369 long-lasting phenotypic alterations that impact their ability to manage challenges. Yet the
370 consequences and mechanisms of previously observed AM training seems quite distinct from
371 that reported herein. For example, administration of live, but not heat-inactivated BCG vaccine
372 resulted in systemic low-grade infection and inflammation that altered gut microbiota
373 composition and increased gut permeability, potentiating AM pro-inflammatory gene expression
374 [36]. In addition, compared to BCG, SFB colonization had a somewhat opposite outcome on AM
375 function in that it suppressed rather than promoted pro-inflammatory gene expression. In further
376 contrast to BCG, phenotypic impacts of SFB were maintained in gnotobiotic mice, arguing
377 against broad changes in microbiota composition playing a central role. Another starkly different
378 example of AM training is the recent observation that IAV infection increases ability of AM to
379 suppress tumors [37]. Such AM training is mediated by a large-scale depletion of AM, which are
380 then replaced by cells newly recruited from bone marrow that, even after establishing residency
381 in the lung, exhibit stark global differences in gene expression profiles. In contrast, SFB
382 colonization phenotypically transformed resident AM without a detectable influx of monocyte

383 precursors. Moreover, gene expression profiling of SFB^- and SFB^+ AM revealed only modest
384 differences, likely reflecting that both SFB^- and SFB^+ AM had been generated by AM self-
385 renewal processes that normally maintain AM homeostasis in non-traumatic states.

386 Despite being modest, SFB-induced changes in basal AM gene expression contributed
387 mightily to the enhanced ability of SFB-colonized mice to manage IAB infection. Most notably,
388 use of *C1qa*$^{-/-}$ mice, and AM transferred therefrom, indicated that SFB-induced increases in C1qa
389 expression were pivotal for lowered viral titers. The comparable genetically-modified mice to
390 similarly examine the necessity of genes that mediated SFB's suppression of AM inflammatory
391 signaling are not yet in hand. However, a converse approach, namely use of a Notch-4
392 neutralizing antibody, argued that the SFB-induced reduction in Notch-4 expression was
393 germane to SFB-induced AM inflammatory anergy and that this aspect of the SFB^+ AM
394 phenotype also contributed to protection against IAV. In addition to directly disabling IAV, AM
395 can also protect lung EC from IAV infection via suppressing EC CysLT1 signaling, which might
396 mediate IAV entry into these cells [24]. Thus, persistence of AM in SFB^+ mice, by itself, likely also
397 contributed to SFB's protection against IAV. That mechanisms driving RVI-induced AM
398 depletion are not clear, makes determining how SFB colonization prevents such depletion
399 challenging. Indeed, deciphering the interrelationships between reduced viral titers,
400 inflammatory anergy, and increased AM survival, is a complex endeavor in which some events
401 are likely both a cause and consequence of each other. For instance, collectively our results
402 indicate that AM persistence enabled them to suppress IAV, but yet such suppression of IAV
403 likely contributed to increased AM survival. Conversely, we envisage that SFB-induced AM
404 inflammatory anergy promoted AM persistence, which in turn enabled sustained protection of
405 epithelial cells from IAV infection. Such protection of epithelial cells from IAV infection would

406 reduce the viral burden, which likely contributes to both inflammation and AM death. Hence,
407 defining the relative contributions of enhanced antiviral and suppressed inflammation is a
408 complex undertaking. Nonetheless, our current working hypothesis is that elevated C1qa
409 expression plays a leading role, and inflammatory anergy plays a key supporting role, in
410 mediating SFB's protection against RVI.

411 Less clear is the nature of the signal that is generated by SFB colonization of the luminal
412 surface of the intestine that drives AM reprogramming. We speculate that SFB produces, or
413 induces host production of, a metabolite(s) that reach the lung and act upon AM, changing both
414 their basal gene expression and how they respond to challenge, perhaps by altering DNA
415 methylation. Additionally/alternatively, it is possible that gut to brain and/or brain to lung neural
416 signaling is involved. We envisage that deciphering how SFB impacts lung AM may yield
417 strategies to mitigate disease burden cause by RVI. Indeed, in addition to mitigating primary
418 RVI, AM persistence may help prevent secondary consequences of RVI. Many of the severe
419 consequences of IAV infection in humans result from secondary bacterial infections, to which
420 the lung is more permissive by loss of IAV-induced AM depletion [38]. Such impaired antibacterial
421 immunity can persist for prolonged periods perhaps reflecting that the bone-marrow derived
422 replacement AM are not quickly optimized for mucosal host defense. Thus, microbiota mediated
423 AM programming may not only influence severity of acute RVI but may also be a long term
424 post-RVI health determinant.
425

Acknowledgments:

We thank Tim Denning and Ifor Williams for insightful guidance. We thank RS Baric for SARS-CoV-2 MA10 virus isolate and Georgia State University's High Containment Core and Division of Animal Resources for support. **Funding**: This work was supported, in part, by Public Health Service grants AI141222 (to RKP), AI171403 (to RKP), and AI170014 (to ATG) from the NIH/NIAID. The funders had no role in study design, data collection and interpretation, or the decision to submit the work for publication.

Author contributions: Conceptualization: RKP, ATG. Investigation: VLN, CML, HK, KS. Resources: RKP, ATG. Visualization: VLN, CML, KS, RKP, ATG. Validation: RKP, ATG. Funding acquisition: RKP. Project administration: RKP, ATG. Supervision: RKP, ATG, MK. Writing – original draft: ATG. Writing – review & editing: VLN, CML, KS, RKP.

Declaration of interest: RKP reports contract testing from Enanta Pharmaceuticals and Atea Pharmaceuticals, and research support from Gilead Sciences, outside of the described work. All other authors declare that they have no competing interests.

Data and materials availability: All data are available in the main text or the supplementary materials.

443 **FIGURE LEGENDS**

444 **Figure 1. Colonization of the intestine with SFB protected mice from influenza virus**
445 **infection.**

446 **(A)** EF and SPF mice were inoculated with A/CA/07/2009 (H1N1) influenza virus (CA09) as
447 schematized. Lung viral titers, survival, bodyweight, and temperature were monitored.

448 **(B)** As schematized, conventionally colonized SFB^- mice received feces that lacked SFB (SFB^-),
449 contained SFB (SFB^+), or contained SFB but no other bacteria (SFB-MA). Seven days post-
450 transplant, mice were inoculated with CA09. Mice were euthanized 4.5-days later or monitored
451 daily for survival, body weight, and temperature for 2 weeks. Statistical analyses were performed
452 with SFB^- as a control group.

453 **(C)** SFB^- mice were administered SFB 3 months or 7 days prior to CA09 inoculation. **(i)** qRT-
454 PCR analysis of SFB colonization level over the course of 14 weeks. **(ii)** Mice were euthanized
455 4.5-days later or monitored daily for survival, body weight, and temperature for 2 weeks.

456 **(D)** qRT-PCR analysis of SFB level in the small intestine, lungs, and spleens after 7 days
457 colonization.

458 **(E)** SFB^- mice were untreated (naive) or administrated SFB. Seven days later, mice were
459 inoculated (or not) with CA09. Mice were euthanized 4.5 days later. H&E staining lung sections
460 scored for pleuritis, bronchiolitis, alveolitis, vasculitis, interstitial pneumonia (IP), and
461 perivascular cuffing (PVC).

462 All experiments n = 5 mice per group. Data is representative of two to three independent
463 experiments. yielding an identical pattern of results. Statistical analyses of survival, bodyweight
464 change, and temperature of (B) and (C) were conducted by comparing "SFB-"or "-SFB" group
465 to all other groups. Statistical analysis; Viral titer: One-way ANOVA or student *t* test. survival:

466 Log-rank Mantel-Cox test. Body weights and temperature: Two-way ANOVA. *p<0.05,
467 **p<0.01, ***p<0.001, ns not significant.
468

469 **Figure 2. SFB mediated protection against IAV was maintained in an array of knockout**
470 **mice and did not require complex gut microbiota.**

471 Lung viral titer, survival rate, body weight change, and temperature of: SFB-negative mice were
472 colonized with SFB for 7 days then inoculated with CA09.

473 **(A)** *rag1*$^{-/-}$ mice

474 **(B)** C57BL/6 mice received neutralization of IL-17/IL-22 monoclonal antibodies every other day
475 throughout the experiment

476 **(C)** *Ifnar*$^{-/-}$ mice

477 **(D)** *rag1*$^{-/-}$*yc*$^{-/-}$ mice

478 **(E)** *stat1*$^{-/-}$ mice

479 **(F)** Altered Schaedler flora (ASF) mice.

480 All experiments n = 5 mice per group. Statistical analysis; Viral titer: student *t* test, Survival:
481 Log-rank Mantel-Cox test. Body weights and temperature: Two-way ANOVA. **p<0.01,
482 ***p<0.001.

483

484 **Figure 3. SFB's protection against IAV infection associated with preservation of resident**
485 **lung phagocytes.**
486 **(A)** SFB$^-$ mice were untreated (naïve) or SFB was administered. Seven days later, mice were
487 inoculated (or not) with CA09. Mice were euthanized 4.5-days later. **(i)** Whole lung gene
488 expression assayed by RNA-seq and data are displayed as heatmap of genes that are significantly
489 altered by 2-fold in all treatment groups relative to the naïve group. **(ii)** Quantitation of CA09
490 level in these extracts by qRT-PCR.
491 **(B)** SFB$^-$ mice were untreated (naïve) or SFB was administered. Seven days later, mice were
492 inoculated (or not) with CA09. Mice were euthanized 4.5-days later, and lung assayed by flow
493 cytometry. **(i & ii)** Analysis of dendritic cells and alveolar macrophage; representative flow plot
494 and frequencies and cell numbers **(i)** cDC1. **(ii)** alveolar macrophages. **(iii)** Frequencies and cell
495 numbers of lung neutrophils, inflammatory monocytes, and NK cells.
496 **(C) (i)** Experimental schema: SFB$^-$ mice colonized with SFB, inoculated with CA09, and treated
497 with 4'-FlU at indicated doses. On day 4.5 post virus inoculation, mice were euthanized, and
498 lungs were harvested to determine virus titers and FACs analysis. **(ii)** lung viral titer. **(iii)** FACs
499 plot graphical representation, frequencies, and cell numbers of lung cDC1, and AMs. **(iv)** Cell
500 numbers of lung neutrophils, inflammatory monocytes, and NK cells.
501 All experiment n = 4-5 per group. Data is representative of two to three independent experiments
502 (B and C), yielding an identical pattern of results. Statistical analysis: One-way ANOVA.
503 *$p<0.05$, **$p<0.01$, ***$p<0.001$, ****$p<0.0001$, ns not significant.
504

505 **Figure 4. SFB-mediated protection against IAV infection and resulting disease required**
506 **alveolar macrophages.**
507 **(A-B) (A)** *batf3*$^{-/-}$ and **(B)** *csf2*$^{-/-}$ mice were administered SFB and then, 7 days later, inoculated
508 with CA09. Lung viral titer, body weight change, temperature, and survival were monitored.
509 **(C) (i-ii)** SFB^{-} mice were orally administered with clodronate liposomes one day before mice
510 were euthanized. FACS analysis to determine the AMs depletion efficacy after clodronate
511 treatment. **(i)** FACS graphical representation of lung AMs, frequency of lung AMs and others
512 immune cells after clodronate treatment. **(ii)** SFB^{-} mice were colonized with SFB for 7 days, and
513 clodronate liposomes were orally administered to mice one day before CA09 inoculation. Mice
514 were euthanized on day 4 post-virus inoculation. Lung viral titer, survival rate, body weight,
515 temperature was measured. Statistical analyses of survival, bodyweight change, and temperature
516 were conducted by comparing "SFB+CA09" group to all other groups.
517 **(D)** SFB^{-} mice were untreated (naïve) or SFB was administered. Seven days later, mice were
518 inoculated (or not) with CA09. Mice were euthanized 4.5-days later. Level of cleaved caspase-3
519 of alveolar macrophages in lung were measured with FACS.
520 **(E-F)** SFB^{-} mice were untreated or treated as in (D). The level of **(E)** CD71 and **(F)** Ki-67
521 expression of alveolar macrophages in the lungs were measured with FACS.
522 **(G)** SFB^{-} mice treated as described in (C) FACS plot graphical representation, and frequencies
523 CA09 level in T1ACEs, T2AECs, and Conducting AECs were assayed by flow cytometry.
524 All experiment n = 5 mice per group. Data is representative of two to three independent
525 experiments (B-F), yielding an identical pattern of results. Statistical analysis; Viral titer, relative
526 SFB genomes, MFI, frequencies/cell numbers of immune cell data: One-way ANOVA or student

527 *t* test. Survival data Log-rank Mantel-Cox. Body weights, temperature: Two-way ANOVA.

528 *$p<0.05$, ***$p<0.001$, ****$p<0.0001$, ns not significant.

529

530 **Figure 5. SFB colonization intrinsically altered AM to withstand IAV-induced depletion.**

531 **(A)** As schematized, SFB^{-} CD45.1 mice were administered with SFB or PBS. Seven days later,
532 AM were isolated by FACs-sorting, and transferred to SFB- CD45.2 mice. One day post-transfer
533 mice were inoculated with CA09. Four days later, lungs were harvested, and AM analyzed by
534 FACs. Representative FACs plots, cell frequencies, cell numbers, and cleaved caspase-3 level
535 are shown.

536 **(B)** SFB^{-} mice were untreated (naïve) or administrated SFB. Seven days later, mice were
537 inoculated (or not) with CA09. Mice were euthanized 4.5-days later. **(i)** qRT-PCR analysis of
538 monocytes chemo-attractants *Ccl2* and *Cxcl10* from lung tissues. **(ii)** Representative FACs plots,
539 cell frequencies, and ratio of tissue residents AM (TR-AM), and monocyte-derived AM (Mo-
540 AM).

541 **(C) (i)** As schematized, AM isolated from CD45.1 mice were transferred to CD45.2 mice. One
542 day post-transferred, mice were administered with SFB or PBS for seven days then mice were
543 inoculated with CA09. For day later, lungs were harvested, and AM analyzed by FACs. **(ii)** Cell
544 numbers are shown.

545 All experiment n = 5 mice per group. Data is representative of two independent experiments (A-
546 B), yielding an identical pattern of results. Statistical test: One-way ANOVA. **$p<0.01$,
547 ***$p<0.001$, ****$p<0.0001$, ns not significant.

548

549 **Figure 6. SFB$^+$ AM exhibited inflammatory anergy and enhanced antiviral function *ex vivo*.**

550 **(A)** Schematic design for *ex vivo* studies of AM.

551 **(B)** Comparison of basal SFB$^+$ and SFB$^-$ AM gene expression by RNA-seq, shown as a volcano
552 plot.

553 **(C)** SFB$^+$ and SFB$^-$ AM were exposed to UV-CA09 with or without Notch4 neutralizing, or
554 isotype control antibodies. RNA was harvested 24 hours later, and gene expression assayed by
555 RT-qPCR shown as a heatmap.

556 **(D)** AM and CA09 stocks were incubated at 37°C, or indicated temperature, for 45 minutes and
557 supernatants were collected. In addition, some cells had new media added and were incubated for
558 another 24 hours. **(i)** Vius infection titers in supernatant at 45 minutes and 24 hours were
559 assayed. **(ii)** Supernatants were collected after 45 minutes incubated with CA09 and viral
560 genomes quantitated by RT-qPCR. **(iii)** Cell-free supernatant of 15 hours AM cultures were
561 incubated with live CA09 stocks, with or without C1qa-neutralization or isotype antibody for 45
562 minutes, at which point virus infection titers were assayed. **(iv)** Cell lysates were generated upon
563 CA09 removal or 24 hours later and viral genomes quantitated by RT-qPCR.

564 **(E)** As schematized, mice were administered with SFB. Seven days later, bronchoalveolar lavage
565 fluid (BALF) and lung were harvested, and AM were isolated via FAC-sorting. C1qa secretions
566 were assayed by ELISA.

567 **(F) (i)** 15 weeks old *C1qa*$^{+/+}$ and *C1qa*$^{-/-}$ SFB$^-$ mice were untreated (naïve) or administrated SFB
568 and then, 7 days later, inoculated with CA09. Mice were euthanized and lungs were harvested
569 4.5-days post CA09 inoculation. **(ii)** Images of lungs. **(iii)** Survival, body weight change,
570 temperature. **(iv)** Lung viral titer. **(v)** Frequencies CA09 level in T1ACEs, T2AECs, and

571 Conducting AECs were assayed by FACs. **(vi)** Gene expression assayed by RT-qPCR shown as
572 a heatmap. **(vii)** Cell numbers of neutrophils, inflammatory monocytes and AM assayed by
573 FACs. Statistical analyses of survival, body weight change, and temperature were conducted
574 between *C1qa*$^{-/-}$ and *Cq1a*$^{-/-}$+SFB group.
575 All experiment n = 4-5 mice per group. Data is representative of two independent experiments,
576 yielding an identical pattern of results. Statistical analysis: One-way ANOVA. *$p<0.05$,
577 **$p<0.01$, ****$p<0.0001$, ns not significant.
578

579 **Figure 7. Adoptive transfer of SFB$^+$ AM enabled recipients to better manage IAV infection.**

580 **(A)** As schematized, SFB$^-$ mice were administered SFB or PBS. Seven days later, AMs were
581 isolated by FACs-sorting and transferred to SFB$^-$ mice. Mice were administered 5x10^5 cells per
582 mouse. One day post adoptive transfer, mice were inoculated with a lethal dose of CA09. Mice
583 were euthanized 4.5 days post-inoculation for viral titer and gross lung assessment or monitored
584 for survival, body weight, and temperature. Statistical analyses of survival, body weight change,
585 and temperature were conducted using the "PBS" group as the control group.
586 **(B)** As schematized, AMs from SFB$^-$ *csf2*$^{+/+}$ mice were administered SFB or PBS. Seven days
587 later, AMs were isolated by FACs-sorting and transferred to SFB$^-$ *csf2*$^{-/-}$ mice. One day post-
588 transfer, mice were inoculated with CA09. Mice were monitored for 14 days for clinical
589 symptoms including survival rate, body weight, and temperature.

590 **(C)** SFB$^-$ mice were administered clodronate liposomes to remove endogenous AM populations.
591 Seven days later after initiation of depletion, mice were administered 5x10^5 AM cells harvested
592 from the SFB$^-$ or SFB$^+$ mice. One day post transfer, mice were inoculated with CA09. Mice were
593 euthanized on day four to assess lung viral titer and gross lung assessment or monitored for
594 survival, body weight, and temperature.

595 All experiments have at least n = 5 mice per group. Data is representative of two independent
596 experiments (A), yielding an identical pattern of results. Statistical analyses of survival,
597 bodyweight change, and temperature of (A-C) were conducted by comparing "PBS" group to all
598 other groups. Statistical analysis; One-way ANOVA: viral titers. Survival: Log-rank Mantel-Cox
599 test. Body weight, temperature: Two-way ANOVA. *$p<0.05$, **$p<0.01$, ****$p<0.0001$, ns not
600 significant.

601

602 **STAR METHODS**
603
604 **RESOURCE AVAILABILITY**

605 **Lead contact**

606 Further information and requests for resources and reagents should be directed to and will be
607 fulfilled by the lead contact, Andrew Gewirtz (agewirtz@gsu.edu).

608 **Materials availability**

609 This study did not generate new unique reagents.

610 **Data and code availability**

611 • The raw sequencing data has been deposited at GenBank with access number:
612 PRJEB71689, and PRJEB71449, and all other data used for this study will be shared upon
613 reasonable request from the lead contact.
614 • This paper does not report original codes.
615 • Any additional information required to reanalyze the data reported in this paper is available
616 from the lead contact upon reasonable request.
617

618 **EXPERIMENTAL MODEL DETAILS**
619

620 **Virus strains and growth conditions**

621 All viruses and cells used in this study are listed in the key resources table. Madin-Darby Canine
622 Kidney (MDCK; ATCC CCL-34), HEp-2 (ATCC CCL-23), and VeroE6 TMPRSS2 (BPS
623 Bioscience #78081) cells were cultured in Dulbecco's Modified Eagle's Medium (DMEM)
624 supplemented with 7.5% heat-inactivated fetal bovine serum (FBS) at 37°C and 5% CO_2. All cell
625 lines used in this study were authenticated and checked for *Mycoplasma* and microbial
626 contamination. Recombinant Influenza A virus was recovered based on original reports for

627 laboratory adapted IAV [39]. A/CA/07/2009 (H1N1) was grown on MDCK cells using serum-free
628 DMEM supplemented with 0.5% Trypsin. Recombinant RSV strain A2 with line19F reporter
629 gene recRSV-mKate was rescued and amplified as described previously [40], and the SARS-CoV-2
630 MA10 strain [41] was passaged in VeroE6 TMPRSS2 cells. All viruses used were clarified,
631 aliquoted, and stored at -80°C. Virus stock titers were determined through $TCID_{50}$-titration.
632

633 **Complex microbiota and mono-associated SFB transplantation**

634 Fecal samples were collected from donor mice, suspended in 20% glycerol PBS solution at 40
635 mg/mL concentration, passed through a 40 µm filter, and stored at -80C. Frozen fecal
636 suspensions were orally administered to recipient mice at 200 µl per mouse.
637

638 **Virus infections**

639 All viruses and mice strains used in this study are listed in the key resources table. The
640 Institutional Animal Care and Use Committee of Georgia State University approved animal
641 studies. All mice, unless otherwise stated, were purchased from The Jackson Laboratory. The
642 Jackson Laboratory does not perform testing for segmented filamentous bacteria (SFB) in mice.
643 Nevertheless, all mice obtained from this vendor were tested and confirmed to be SFB-negative
644 upon their arrival at GSU. The following mice were purchased from Taconic Biosciences:
645 C57BL/6 (B6 WT) Excluded Flora (EF) mice and Specific Pathogen-Free (SFP) mice, which we
646 verified were SFB+ and SFB-, respectively. Unless otherwise stated, mice were 5 weeks of age
647 at the time of infection. Upon arrival, mice were acclimated for five days and then randomly
648 assigned to study groups and housed under ABSL-2 or ABSL-3 conditions for infections with
649 A/CA/07/2009 (H1N1) recombinant, recRSV-mKate, or SARS-CoV-2 MA10 strain,
650 respectively. Seven days prior to virus infection, mice were subjected to microbiota manipulation

651 (administration of feces from SPF or SFB-monoassociated mice). Bodyweight was determined
652 twice daily, and body temperature determined once daily rectally. For infections, animals were
653 anesthetized with isoflurane [rec A/CA/07/2009 (H1N1) (CA09)] or ketamine/xylazine (recRSV-
654 mKate and MA-SARS-CoV-2), followed by intranasal inoculation with 2.5×10^2- 2×10^4 $TCID_{50}$
655 units/animal of GFP-expressing reporter virus version of A/CA/07/2009 (H1N1) (CA09),
656 5.5×10^5 of recRSV-mKate, or 4.2×10^5 of MA-SARS-CoV-2. In all cases, virus inoculum was
657 diluted in 50 µl and administered in amounts of 25 µl per nare, followed by treatment with 4'-
658 FlU at specified dose levels and starting time points through oral gavage. Each individual study
659 contained animals receiving equal volumes of vehicle through oral gavage. Animals were
660 euthanized and organs harvested at predefined time points or when animals reached humane
661 study endpoints. At study end point, lung tissue was harvested for virus titration or
662 histopathology.
663
664 **METHODS DETAILS**
665
666 **PCR primers, FACs antibodies, neutralization antibodies and other reagents**
667 All reagents used in these manuscripts can be seen in the key resources table.
668
669 **Histopathologic analysis**
670 Lungs were perfused using 10% neutral-buffered formalin, dissected, and fixed. Formalin-fixed
671 lungs were transferred to 70% EtOH, embedded in paraffin, sectioned, stained, and scored by a
672 board-certified veterinary pathologist (KS), who was blinded to the study groups. For each
673 parameter, the most severe lesion in the section was scored. Pleuritis, bronchiolitis, and alveolitis

674 scoring was based on distribution: 1 = focal, 2 = multifocal, 3 = multifocal to coalescing, 4 =
675 diffuse. For interstitial pneumonia (IP): 1 = alveolar septa expanded by 1 leukocyte thickness, 2
676 = 2-leukocytes thick, 3 = 3-leukocytes thick, 4 = 4-leukocytes thick. For vasculitis: 1 = vessel
677 wall infiltrated by leukocytes, 2 = infiltration and separation of myocytes, 3 = same changes as in
678 2 with fibrinoid change. For perivascular cuffing (PVC): 1 = vessels surrounded by 1 leukocyte
679 layer, 2 = 2 to 5-leukocytes thick, 3 = 6 to 10-leukocytes thick, 4 = more than 10-leukocytes
680 thick.
681
682 **Virus titration**
683 Virus samples were serially diluted (10-fold starting at 1:10 initial dilution) in serum-free
684 DMEM (recRSV-mKate and MA-SARS-CoV-2) and supplemented with 0.5% Trypsin (Gibco,
685 recA/California/07/2009). Serial dilutions were added to cells seeded in 96-well plate at
686 1×10^4 cells per well, 24 hours before infection. Infected plates were incubated for 72 hours at
687 37°C with 5% CO_2 and scoring of wells based on reporter activity/syncytia.
688
689 **Virus titration from tissue samples**
690 Organs were weighed and homogenized in 300 µl PBS using a bead, set to 3 cycles of 30
691 seconds each at 4°C, separated by 30-second rest periods. Homogenates were cleared (10
692 minutes at 20,000 × g and 4°C), and cleared supernatants were stored at -80°C until virus
693 titration. Viral titers were expressed as $TCID_{50}$ units per gram input tissue.
694
695 **Neutralization of IL-17 and IL-22**

696 IL-17 (100 μg) and IL-22 (150 μg) neutralizing monoclonal antibody were administered
697 intraperitoneally before microbiota transplantation and virus inoculation thereafter every other
698 day until mice were euthanized.
699
700 **Lung digestion and flow cytometry analysis/isolation of innate immune cells**
701 Lungs were dissected from mice and finely minced with scissors before digestion (40 minutes, at
702 37ºC) with warm RPMI containing 10% FBS, DNase, and 1mg/mL Collagenase type IV
703 (Sigma); lungs were further homogenized via swishing with a 3-mL syringe every 10 minutes
704 during digestion. Following digestion, immune cells were purified with 40%/80% isotonic Percol
705 gradient centrifugation. For flow cytometry analysis, the prepared cells were blocked with 1
706 μg/million cells with 2.4G2 (anti-CD16/anti-CD32) in 100 μL PBS for 15 minutes at 4ºC,
707 followed by 2-times wash with PBS to remove residue of 2.4G2 and then incubated in
708 conjugated mAbs CD45 BV605, MHCII BV650, CD11b APC-Cy7, CD11c BV786, Ly6C
709 PerCp-Cy5.5, Ly6G AF700, CD64 BV421, CD24 FITC, CD117 GV510, SiglecF PE-CF594,
710 Fcer1 APC. Intracellular staining for cleaved caspase-3 was done using FoxP3 staining buffer
711 purchased from eBioscience. Multi-parameter analysis was performed on a CytoFlex (Beckman
712 Coulter) and analyzed with FlowJo software (Tree Star). Cell sorting was done using Sony
713 SH800Z cell sorter (Sony). Gating strategy for innate immune cells was based on Yu *et al*., [42]
714 and gating strategy for airway epithelial cells was based on Cardani *et al*., [24]. Immune cells and
715 lung airway epithelial subtypes are defined in Table S1.
716
717 **RNA-Seq**
718 RNA was isolated from lungs or FACs-sorted alveolar macrophages using RNeasy Plus Mini Kit
719 from Qiagen. The prepared RNA samples were then sent to the Molecular Evolution Core of

720 Georgia Institute of Technology for library preparation and sequencing on the NextSeq
721 instrument with a high output 2x75bp run. FASTQC was used for sequencing reads quality
722 screening. The RNAseq data were then analyzed using the Galaxy server.
723
724 **Adoptive transfer of alveolar macrophages**
725 Lungs were harvested from CD45.1 mice and digested with Collagenase type IV as described
726 above. Alveolar macrophages (defined at $CD45^{+}MHCII^{+}CD11c^{+}Siglect^{+}$) were stained and
727 FACs-sorted. Small aliquot of isolated cells was used to determined purity. Unless stated
728 otherwise, $5x10^{5}$ alveolar macrophages in 30 µl PBS were administered intranasally to recipient
729 mice. One day post cells transfer, some mice were euthanized to determine transfer efficiency
730 and survival of transferred cells; and some mice were inoculated with IAV. For survival
731 experiments, mice were monitored twice daily for 14 days. For lung virus titers, mice were
732 euthanized on day 4.5 post virus inoculation.
733
734 ***Ex vivo* inhibiting Notch-4 signaling in alveolar macrophages.**
735 Alveolar macrophages were FACS-sorted as described. After sorting, cells were treated with
736 either isotype control antibody (Cat# BE0091, BioXCell) or an anti-Notch4 monoclonal antibody
737 (20µg/mL) (Cat# BE0129, BioXCell), known to neutralize Notch-4 [27] for 30 minutes. Cells
738 were washed twice and resuspended in PBS and intranasally transferred to mice.
739
740 ***Ex vivo* alveolar macrophages culture, virucidal assay, and anti-body mediated removal of**
741 **C1qa.** Alveolar macrophages were FACS-sorted as described. After sorted cells were incubated
742 for 18h at 37°C. Cells were washed twice with serum-free media and were incubated with live
743 CA09 (MOI = 1) in serum-free DMEM supplemented with 0.5% Trypsin (flu media) for 45min.

744 In addition, to assess whether alveolar macrophages are the terminal destination for IAV, some
745 cells had new flu media added and were incubated for another 24h. Viral titer and genomes were
746 determined via $TCID_{50}$ and PCR methods. **Antibody-mediated removal of C1qa from *ex vivo***
747 **alveolar macrophages' supernatants.** Cell-free supernatants of 18h AM cultures were treated
748 with C1qa polyclonal antibodies or isotype for 2 hours at 4ºC and protein A/G was added and
749 centrifuged. Supernatant was harvested and incubated with CA09 stocks for 45mins, at which
750 point IAV infection titers were assayed.
751
752 **Alveolar macrophages phagocytosis assay.** *Ex Vivo* alveolar AM bead uptake assay was
753 performed with Phagocytosis assay kit (Cat#500290, Cayman chemical). Alveolar macrophages
754 were FACS-sorted as described. After sorting, $1x10^5$ cells were seeded in each well of a 96-well
755 plate and incubated for 18h at 37ºC. Cells were washed twice, and IgG-FITC beads were added
756 and incubated for 2 hours at 37ºC. After incubation period, cells were centrifuged, and
757 supernatants were removed and resuspended FACS buffer. Level of cell fluorescence, an
758 indicator of bead uptake, was measured via flow cytometry. For *In vivo* AM bioparticle uptake,
759 SFB^- and SFB^+ mice were administered pHrodo™ *E.coli* BioParticles™ conjugated (Cat#
760 P35360, Invitrogen). Three hours later, mice were euthanized and BALF were harvested, and
761 AM were labeled. Level of cell fluorescence, an indicator of bioparticle uptake, was measured
762 via flow cytometry.
763
764 **Quantitative real-time PCR**
765 Total RNA from lungs or from FACs-sorted alveolar macrophages were isolated using the
766 Qiagen RNeasy Mini Kit with on-column DNase digestion according to manufacturer's protocol.

767 cDNA was generated using the Superscript First Strand Synthesis kit for RT-PCR and random
768 hexamer primers (Invitrogen). RT-qPCR was performed with SYBR Green using StepOnePlus
769 PCR system (Applied Biosystem), and all genes expression was normalized to GAPDH.
770
771 **C1qa ELISA**
772 BALF was collected from SFB^+ and SFB^- mice. Alveolar macrophages (AM) were sorted using
773 fluorescence-activated cell sorting (FACS) from lung and BALF of SFB^+ and SFB^- mice. Sorted
774 AM were incubated in RPMI + 10% FBS overnight at 37°C in a cell culture incubator. BALF
775 and supernatants from cultured AM were coated onto 96-well ELISA plates and incubated
776 overnight at 4°C. Plates were washed with PBST to remove unbound material. Blocking was
777 performed with 3% bovine serum albumin (BSA) in PBS at room temperature for one hour.
778 Polyclonal antibody against C1qa was diluted at 1:5000 and added to the plate and incubated for
779 2h at room temperature. Secondary antibodies (conjugated to horseradish peroxidase, HRP) were
780 added and incubated at room temperature for 1 hour. Tetramethylbenzidine (TMB) substrate was
781 added to detect HRP enzyme conjugate activity. Absorbance at 450 nm was measured to quantify
782 the presence of C1qa. Mouse C1qa recombinant protein was serially diluted to construct a
783 standard curve for determining the concentration of C1qa in the samples. Absorbance values of
784 the samples were compared with the standard curve to determine the concentration of C1qa in
785 the BALF and cultured AM supernatants.
786
787 **AM metabolic assay.**
788 The real-time metabolism of AM was assessed using the Seahorse XF Cell Mito Stress Test Kit
789 or the Seahorse XF Glycolytic Stress Test Kit from Agilent Technologies, following the

790 manufacturer's instructions. AM were FACS-sorted from SFB^+ and SFB^- mice. The sorted cells
791 were then seeded into Seahorse cell culture plates at a density of $1x10^5$ cells per well and
792 cultured overnight in complete RPMI1640 medium. On the following day, AM were incubated
793 with Seahorse assay medium (Agilent Technologies) for one hour. For the glycolysis stress test,
794 AM were supplemented with 2mM glutamine. For the mito stress test, AM were supplemented
795 with 10mM glucose and 1mM pyruvate. All reagents provided in the kits were resuspended in
796 assay medium, and the final concentrations in the culture wells were as follows: 1.5 μM
797 oligomycin, 4 μM FCCP, and 0.5 μM rotenone/antimycin A for the mito stress test, and 10 mM
798 glucose, 1 μM oligomycin, and 50 mM 2-deoxy-D-glucose (2-DG) for the glycolytic stress test.
799 The oxygen consumption rate (OCR) and extracellular acidification rate (ECAR) were measured
800 on a Seahorse XF analyzer. Non-glycolytic ECAR is calculated as the average ECAR values
801 after 2-DG treatment. Basal glycolysis is calculated as the average ECAR value prior to
802 oligomycin treatment minus non-glycolytic ECAR. Max glycolysis is calculated as the average
803 ECAR values after oligomycin and before FCCP treatment. Glycolytic reserve is calculated as
804 max glycolysis minus basal glycolysis. Basal respiration is calculated as the average OCR value
805 prior to oligomycin treatment minus non-mitochondrial OCR. Max respiration is calculated as
806 the average OCR value after FCCP and before rotenone/antimycin A addition.
807
808 **Experimental schematics and graphical abstract.**
809 All experimental schematics and graphical abstract created using BioRender.
810 https://biorender.com/
811
812 **Quantification and statistical analysis**

Results were expressed as mean ± SEM. All data was plotted in GraphPad Prism version 10. Statistical significance was assessed by One-way ANOVA, Student's t test, and Two-way ANOVA. Differences between experimental groups were considered significant if *$p<0.05$, **$p<0.01$, ***$p<0.001$, ****$p<0.0001$.

818 **References**

819 1. Ngo, V.L., and Gewirtz, A.T. (2021). Microbiota as a potentially-modifiable factor influencing
820 COVID-19. Curr Opin Virol *49*, 21-26. 10.1016/j.coviro.2021.04.005.
821 2. Brodin, P. (2022). Immune-microbe interactions early in life: A determinant of health and
822 disease long term. Science *376*, 945-950. 10.1126/science.abk2189.
823 3. Beura, L.K., Hamilton, S.E., Bi, K., Schenkel, J.M., Odumade, O.A., Casey, K.A., Thompson, E.A.,
824 Fraser, K.A., Rosato, P.C., Filali-Mouhim, A., et al. (2016). Normalizing the environment
825 recapitulates adult human immune traits in laboratory mice. Nature *532*, 512-516.
826 10.1038/nature17655.
827 4. Rosshart, S.P., Vassallo, B.G., Angeletti, D., Hutchinson, D.S., Morgan, A.P., Takeda, K., Hickman,
828 H.D., McCulloch, J.A., Badger, J.H., Ajami, N.J., et al. (2017). Wild Mouse Gut Microbiota
829 Promotes Host Fitness and Improves Disease Resistance. Cell *171*, 1015-1028 e1013.
830 10.1016/j.cell.2017.09.016.
831 5. Phelan, J. (2016). Choosing a Health Standard for Your Model.
832 https://www.taconic.com/taconic-insights/quality/choosing-rodent-model-health-
833 standards.html.
834 6. Korth, M.J., Tchitchek, N., Benecke, A.G., and Katze, M.G. (2013). Systems approaches to
835 influenza-virus host interactions and the pathogenesis of highly virulent and pandemic viruses.
836 Semin Immunol *25*, 228-239. 10.1016/j.smim.2012.11.001.
837 7. Ivanov, II, and Littman, D.R. (2010). Segmented filamentous bacteria take the stage. Mucosal
838 Immunol *3*, 209-212. 10.1038/mi.2010.3.
839 8. Teng, F., Klinger, C.N., Felix, K.M., Bradley, C.P., Wu, E., Tran, N.L., Umesaki, Y., and Wu, H.J.
840 (2016). Gut Microbiota Drive Autoimmune Arthritis by Promoting Differentiation and Migration
841 of Peyer's Patch T Follicular Helper Cells. Immunity *44*, 875-888. 10.1016/j.immuni.2016.03.013.

842 9. Shi, Z., Zou, J., Zhang, Z., Zhao, X., Noriega, J., Zhang, B., Zhao, C., Ingle, H., Bittinger, K., Mattei,
843 L.M., et al. (2019). Segmented Filamentous Bacteria Prevent and Cure Rotavirus Infection. Cell
844 *179*, 644-658 e613. 10.1016/j.cell.2019.09.028.
845 10. Zemlin, M., Hummel, M., Anagnostopoulos, I., and Stein, H. (1998). Improved polymerase chain
846 reaction detection of clonally rearranged T-cell receptor beta chain genes. Diagn Mol Pathol *7*,
847 138-145. 10.1097/00019606-199806000-00003.
848 11. Wymore Brand, M., Wannemuehler, M.J., Phillips, G.J., Proctor, A., Overstreet, A.M., Jergens,
849 A.E., Orcutt, R.P., and Fox, J.G. (2015). The Altered Schaedler Flora: Continued Applications of a
850 Defined Murine Microbial Community. ILAR J *56*, 169-178. 10.1093/ilar/ilv012.
851 12. Newton, A.H., Cardani, A., and Braciale, T.J. (2016). The host immune response in respiratory
852 virus infection: balancing virus clearance and immunopathology. Semin Immunopathol *38*, 471-
853 482. 10.1007/s00281-016-0558-0.
854 13. Purnama, C., Ng, S.L., Tetlak, P., Setiagani, Y.A., Kandasamy, M., Baalasubramanian, S.,
855 Karjalainen, K., and Ruedl, C. (2014). Transient ablation of alveolar macrophages leads to
856 massive pathology of influenza infection without affecting cellular adaptive immunity. Eur J
857 Immunol *44*, 2003-2012. 10.1002/eji.201344359.
858 14. Lieber, C.M., Aggarwal, M., Yoon, J.J., Cox, R.M., Kang, H.J., Sourimant, J., Toots, M., Johnson,
859 S.K., Jones, C.A., Sticher, Z.M., et al. (2023). 4'-Fluorouridine mitigates lethal infection with
860 pandemic human and highly pathogenic avian influenza viruses. PLoS Pathog *19*, e1011342.
861 10.1371/journal.ppat.1011342.
862 15. Sourimant, J., Lieber, C.M., Aggarwal, M., Cox, R.M., Wolf, J.D., Yoon, J.J., Toots, M., Ye, C.,
863 Sticher, Z., Kolykhalov, A.A., et al. (2022). 4'-Fluorouridine is an oral antiviral that blocks
864 respiratory syncytial virus and SARS-CoV-2 replication. Science *375*, 161-167.
865 10.1126/science.abj5508.

866 16. Schneider, C., Nobs, S.P., Heer, A.K., Kurrer, M., Klinke, G., van Rooijen, N., Vogel, J., and Kopf,
867 M. (2014). Alveolar macrophages are essential for protection from respiratory failure and
868 associated morbidity following influenza virus infection. PLoS Pathog *10*, e1004053.
869 10.1371/journal.ppat.1004053.
870 17. Dranoff, G., Crawford, A.D., Sadelain, M., Ream, B., Rashid, A., Bronson, R.T., Dickersin, G.R.,
871 Bachurski, C.J., Mark, E.L., Whitsett, J.A., and et al. (1994). Involvement of granulocyte-
872 macrophage colony-stimulating factor in pulmonary homeostasis. Science *264*, 713-716.
873 10.1126/science.8171324.
874 18. Thepen, T., Van Rooijen, N., and Kraal, G. (1989). Alveolar macrophage elimination in vivo is
875 associated with an increase in pulmonary immune response in mice. J Exp Med *170*, 499-509.
876 10.1084/jem.170.2.499.
877 19. Rauschmeier, R., Gustafsson, C., Reinhardt, A., N, A.G., Tortola, L., Cansever, D., Subramanian, S.,
878 Taneja, R., Rossner, M.J., Sieweke, M.H., et al. (2019). Bhlhe40 and Bhlhe41 transcription factors
879 regulate alveolar macrophage self-renewal and identity. EMBO J *38*, e101233.
880 10.15252/embj.2018101233.
881 20. Behar, S.M., Martin, C.J., Booty, M.G., Nishimura, T., Zhao, X., Gan, H.X., Divangahi, M., and
882 Remold, H.G. (2011). Apoptosis is an innate defense function of macrophages against
883 Mycobacterium tuberculosis. Mucosal Immunol *4*, 279-287. 10.1038/mi.2011.3.
884 21. Allden, S.J., Ogger, P.P., Ghai, P., McErlean, P., Hewitt, R., Toshner, R., Walker, S.A., Saunders, P.,
885 Kingston, S., Molyneaux, P.L., et al. (2019). The Transferrin Receptor CD71 Delineates
886 Functionally Distinct Airway Macrophage Subsets during Idiopathic Pulmonary Fibrosis. Am J
887 Respir Crit Care Med *200*, 209-219. 10.1164/rccm.201809-1775OC.

888 22. Kuczma, M.P., Szurek, E.A., Cebula, A., Chassaing, B., Jung, Y.J., Kang, S.M., Fox, J.G., Stecher, B.,
889 and Ignatowicz, L. (2020). Commensal epitopes drive differentiation of colonic T(regs). Sci Adv *6*,
890 eaaz3186. 10.1126/sciadv.aaz3186.
891 23. Ruan, T., Sun, J., Liu, W., Prinz, R.A., Peng, D., Liu, X., and Xu, X. (2020). H1N1 Influenza Virus
892 Cross-Activates Gli1 to Disrupt the Intercellular Junctions of Alveolar Epithelial Cells. Cell Rep *31*,
893 107801. 10.1016/j.celrep.2020.107801.
894 24. Cardani, A., Boulton, A., Kim, T.S., and Braciale, T.J. (2017). Alveolar Macrophages Prevent Lethal
895 Influenza Pneumonia By Inhibiting Infection Of Type-1 Alveolar Epithelial Cells. PLoS Pathog *13*,
896 e1006140. 10.1371/journal.ppat.1006140.
897 25. Misharin, A.V., Morales-Nebreda, L., Mutlu, G.M., Budinger, G.R., and Perlman, H. (2013). Flow
898 cytometric analysis of macrophages and dendritic cell subsets in the mouse lung. Am J Respir
899 Cell Mol Biol *49*, 503-510. 10.1165/rcmb.2013-0086MA.
900 26. Berrebi, D., Bruscoli, S., Cohen, N., Foussat, A., Migliorati, G., Bouchet-Delbos, L., Maillot, M.C.,
901 Portier, A., Couderc, J., Galanaud, P., et al. (2003). Synthesis of glucocorticoid-induced leucine
902 zipper (GILZ) by macrophages: an anti-inflammatory and immunosuppressive mechanism shared
903 by glucocorticoids and IL-10. Blood *101*, 729-738. 10.1182/blood-2002-02-0538.
904 27. Xia, M., Harb, H., Saffari, A., Sioutas, C., and Chatila, T.A. (2018). A Jagged 1-Notch 4 molecular
905 switch mediates airway inflammation induced by ultrafine particles. J Allergy Clin Immunol *142*,
906 1243-1256 e1217. 10.1016/j.jaci.2018.03.009.
907 28. Varghese, P.M., Kishore, U., and Rajkumari, R. (2022). Human C1q Regulates Influenza A Virus
908 Infection and Inflammatory Response via Its Globular Domain. Int J Mol Sci *23*.
909 10.3390/ijms23063045.

910 29. Klickstein, L.B., Barbashov, S.F., Liu, T., Jack, R.M., and Nicholson-Weller, A. (1997). Complement
911 receptor type 1 (CR1, CD35) is a receptor for C1q. Immunity *7*, 345-355. 10.1016/s1074-
912 7613(00)80356-8.
913 30. Smythies, L.E., Sellers, M., Clements, R.H., Mosteller-Barnum, M., Meng, G., Benjamin, W.H.,
914 Orenstein, J.M., and Smith, P.D. (2005). Human intestinal macrophages display profound
915 inflammatory anergy despite avid phagocytic and bacteriocidal activity. J Clin Invest *115*, 66-75.
916 10.1172/JCI19229.
917 31. Abt, M.C., Osborne, L.C., Monticelli, L.A., Doering, T.A., Alenghat, T., Sonnenberg, G.F., Paley,
918 M.A., Antenus, M., Williams, K.L., Erikson, J., et al. (2012). Commensal bacteria calibrate the
919 activation threshold of innate antiviral immunity. Immunity *37*, 158-170.
920 10.1016/j.immuni.2012.04.011.
921 32. Ichinohe, T., Pang, I.K., Kumamoto, Y., Peaper, D.R., Ho, J.H., Murray, T.S., and Iwasaki, A. (2011).
922 Microbiota regulates immune defense against respiratory tract influenza A virus infection. Proc
923 Natl Acad Sci U S A *108*, 5354-5359. 10.1073/pnas.1019378108.
924 33. Chen, H., Wang, L., Wang, X., Wang, X., Liu, H., and Yin, Y. (2020). Distribution and Strain
925 Diversity of Immunoregulating Segmented Filamentous Bacteria in Human Intestinal Lavage
926 Samples. Microb Ecol *79*, 1021-1033. 10.1007/s00248-019-01441-4.
927 34. Jonsson, H., Hugerth, L.W., Sundh, J., Lundin, E., and Andersson, A.F. (2020). Genome sequence
928 of segmented filamentous bacteria present in the human intestine. Commun Biol *3*, 485.
929 10.1038/s42003-020-01214-7.
930 35. Subramanian, S., Busch, C.J., Molawi, K., Geirsdottir, L., Maurizio, J., Vargas Aguilar, S., Belahbib,
931 H., Gimenez, G., Yuda, R.A.A., Burkon, M., et al. (2022). Long-term culture-expanded alveolar
932 macrophages restore their full epigenetic identity after transfer in vivo. Nat Immunol *23*, 458-
933 468. 10.1038/s41590-022-01146-w.

934 36. Jeyanathan, M., Vaseghi-Shanjani, M., Afkhami, S., Grondin, J.A., Kang, A., D'Agostino, M.R., Yao,
935 Y., Jain, S., Zganiacz, A., Kroezen, Z., et al. (2022). Parenteral BCG vaccine induces lung-resident
936 memory macrophages and trained immunity via the gut-lung axis. Nat Immunol *23*, 1687-1702.
937 10.1038/s41590-022-01354-4.
938 37. Wang, T., Zhang, J., Wang, Y., Li, Y., Wang, L., Yu, Y., and Yao, Y. (2023). Influenza-trained
939 mucosal-resident alveolar macrophages confer long-term antitumor immunity in the lungs. Nat
940 Immunol *24*, 423-438. 10.1038/s41590-023-01428-x.
941 38. Verma, A.K., Bansal, S., Bauer, C., Muralidharan, A., and Sun, K. (2020). Influenza Infection
942 Induces Alveolar Macrophage Dysfunction and Thereby Enables Noninvasive Streptococcus
943 pneumoniae to Cause Deadly Pneumonia. J Immunol *205*, 1601-1607.
944 10.4049/jimmunol.2000094.
945 39. Nogales, A., Avila-Perez, G., Rangel-Moreno, J., Chiem, K., DeDiego, M.L., and Martinez-Sobrido,
946 L. (2019). A Novel Fluorescent and Bioluminescent Bireporter Influenza A Virus To Evaluate Viral
947 Infections. J Virol *93*. 10.1128/JVI.00032-19.
948 40. Hotard, A.L., Shaikh, F.Y., Lee, S., Yan, D., Teng, M.N., Plemper, R.K., Crowe, J.E., Jr., and Moore,
949 M.L. (2012). A stabilized respiratory syncytial virus reverse genetics system amenable to
950 recombination-mediated mutagenesis. Virology *434*, 129-136. 10.1016/j.virol.2012.09.022.
951 41. Dinnon, K.H., 3rd, Leist, S.R., Schafer, A., Edwards, C.E., Martinez, D.R., Montgomery, S.A., West,
952 A., Yount, B.L., Jr., Hou, Y.J., Adams, L.E., et al. (2020). A mouse-adapted model of SARS-CoV-2 to
953 test COVID-19 countermeasures. Nature *586*, 560-566. 10.1038/s41586-020-2708-8.
954 42. Yu, Y.R., O'Koren, E.G., Hotten, D.F., Kan, M.J., Kopin, D., Nelson, E.R., Que, L., and Gunn, M.D.
955 (2016). A Protocol for the Comprehensive Flow Cytometric Analysis of Immune Cells in Normal
956 and Inflamed Murine Non-Lymphoid Tissues. PLoS One *11*, e0150606.
957 10.1371/journal.pone.0150606.

Figure 1

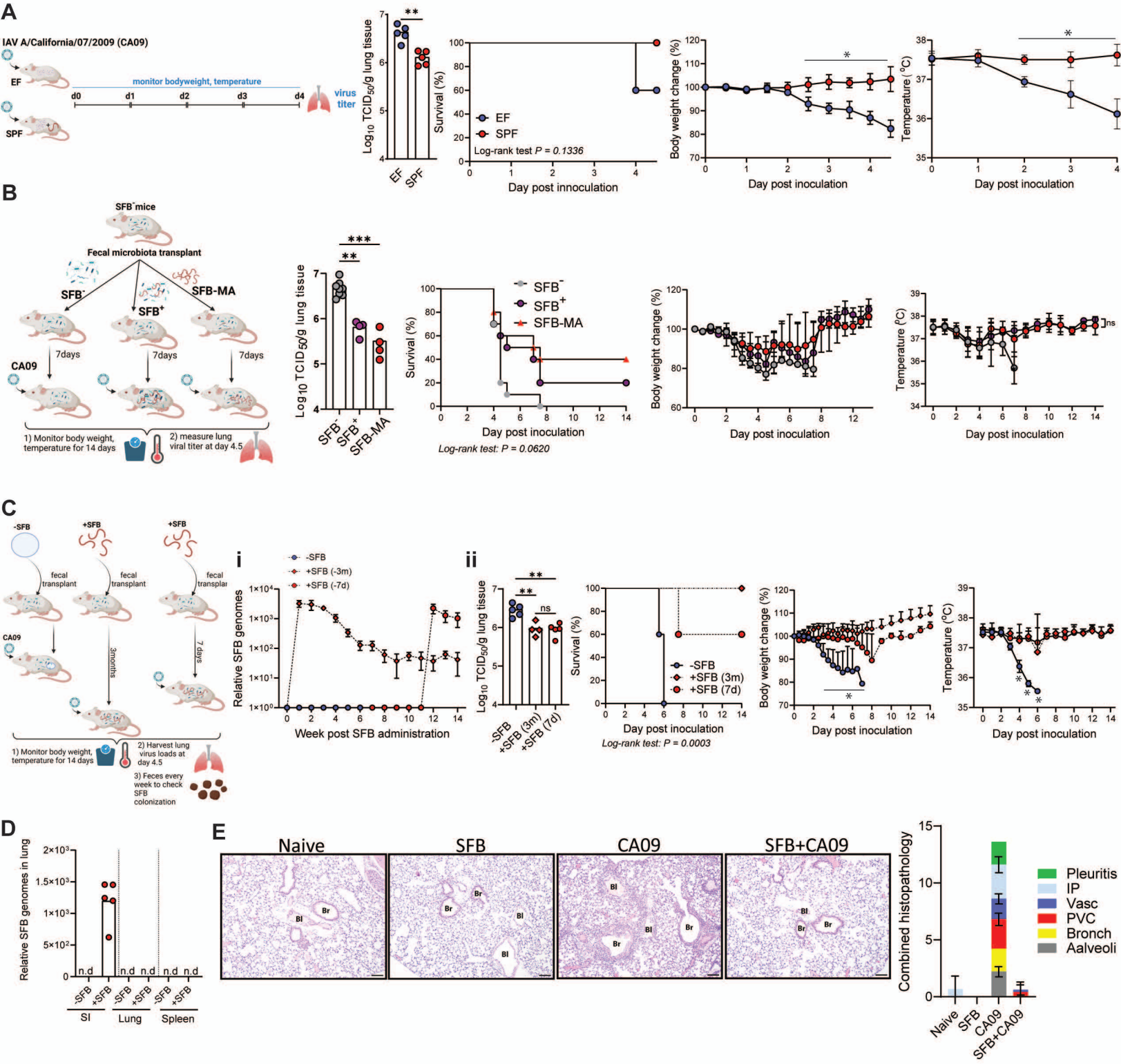
A
IAV A/California/07/2009 (CA09)
EF
SPF
monitor bodyweight, temperature
d0
d1
d2
d3
d4
virus titer
Log10 TCID50/g lung tissue
EF
SPF
Survival (%)
Log-rank test P = 0.1336
Day post innoculation
Body weight change (%)
Day post inoculation
Temperature (°C)
Day post inoculation
B
SFB⁻mice
Fecal microbiota transplant
SFB⁻
SFB⁺
SFB-MA
7days
CA09
1) Monitor body weight, temperature for 14 days
2) measure lung viral titer at day 4.5
Log10 TCID50/g lung tissue
SFB⁻
SFB⁺
SFB-MA
Survival (%)
Log-rank test: P = 0.0620
Day post inoculation
Body weight change (%)
Day post inoculation
Temperature (°C)
Day post inoculation
C
-SFB
+SFB
fecal transplant
CA09
3months
7 days
1) Monitor body weight, temperature for 14 days
2) Harvest lung virus loads at day 4.5
3) Feces every week to check SFB colonization
i
-SFB
+SFB (-3m)
+SFB (-7d)
Relative SFB genomes
Week post SFB administration
ii
Log10 TCID50/g lung tissue
-SFB
+SFB (3m)
+SFB (7d)
Survival (%)
Log-rank test: P = 0.0003
Day post inoculation
Body weight change (%)
Day post inoculation
Temperature (°C)
Day post inoculation
D
Relative SFB genomes in lung
n.d
-SFB
+SFB
SI
Lung
Spleen
E
Naive
SFB
CA09
SFB+CA09
Bl
Br
Combined histopathology
Pleuritis
IP
Vasc
PVC
Bronch
Aalveoli
Naive
SFB
CA09
SFB+CA09

Figure 2

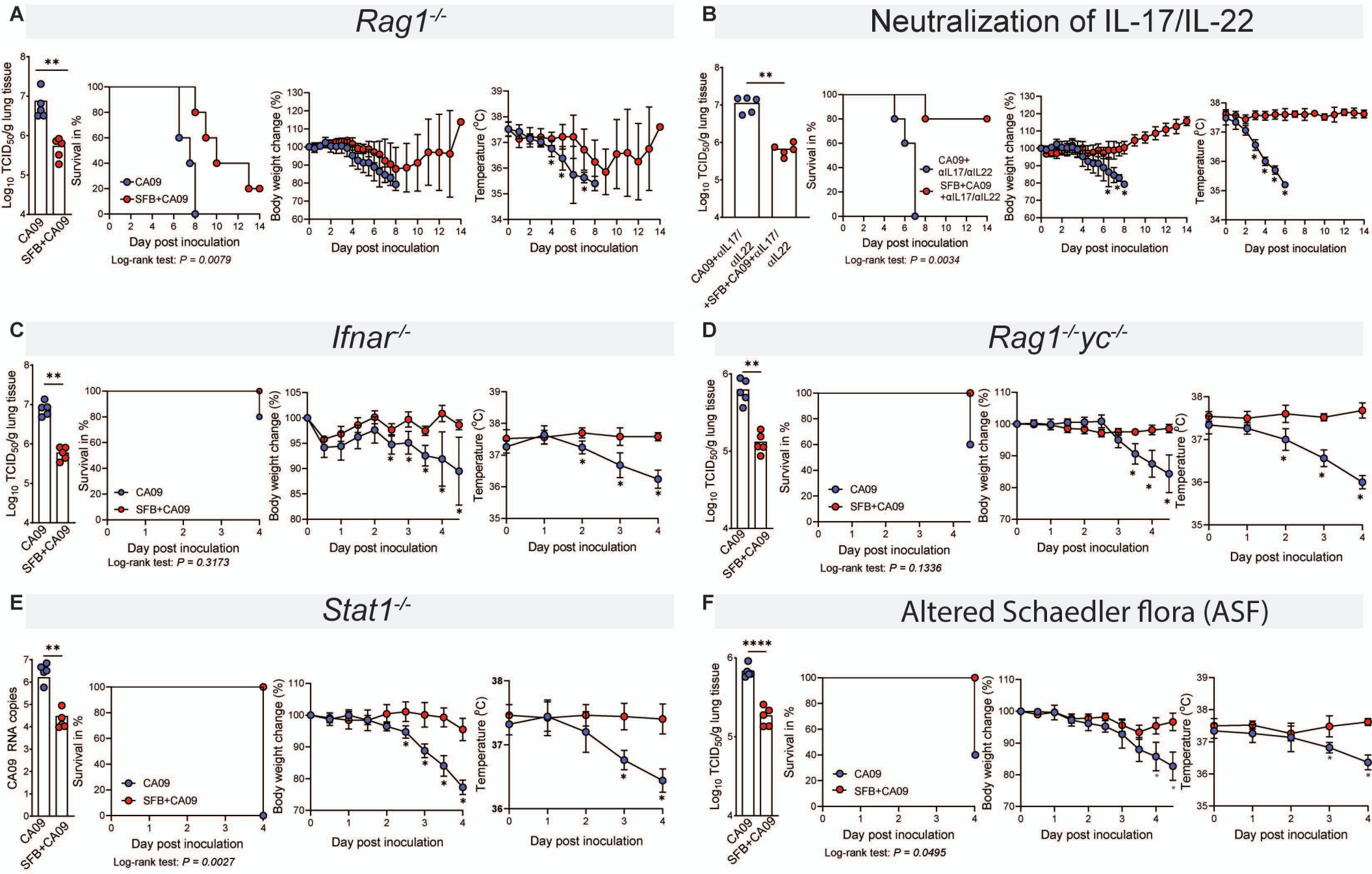
A
Rag1-/-
B
Neutralization of IL-17/IL-22
C
Ifnar-/-
D
Rag1-/-yc-/-
E
Stat1-/-
F
Altered Schaedler flora (ASF)
Log10 TCID50/g lung tissue
CA09 RNA copies
Survival in %
Body weight change (%)
Temperature (°C)
Day post inoculation
CA09
SFB+CA09
CA09+αIL17/αIL22
SFB+CA09 +αIL17/αIL22
Log-rank test: P = 0.0079
Log-rank test: P = 0.0034
Log-rank test: P = 0.3173
Log-rank test: P = 0.1336
Log-rank test: P = 0.0027
Log-rank test: P = 0.0495

Figure 3

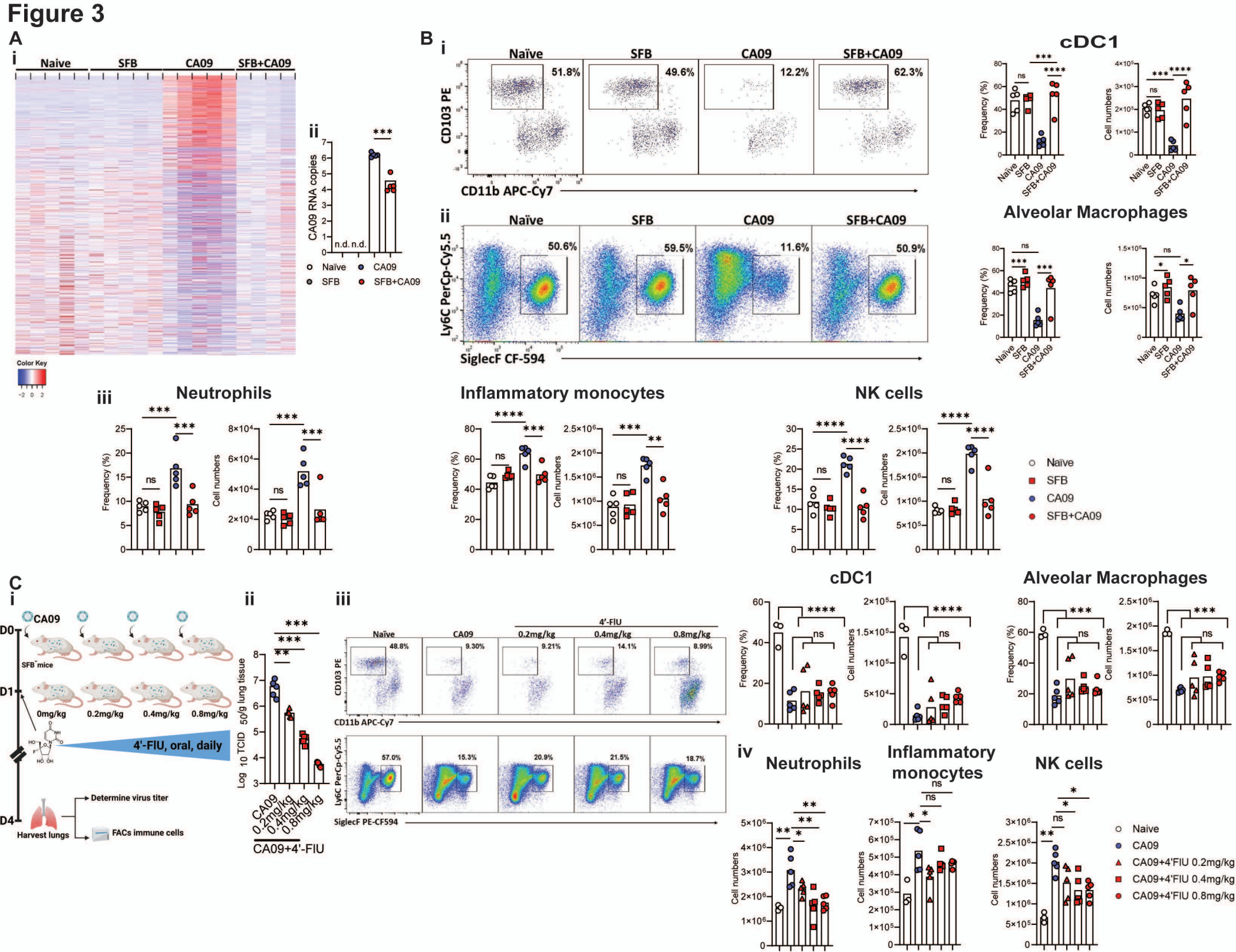
A
i
Naive
SFB
CA09
SFB+CA09
Color Key
ii
CA09 RNA copies
n.d. n.d.
Naïve
CA09
SFB
SFB+CA09
B
i
Naïve
SFB
CA09
SFB+CA09
51.8%
49.6%
12.2%
62.3%
CD103 PE
CD11b APC-Cy7
ii
50.6%
59.5%
11.6%
50.9%
Ly6C PerCp-Cy5.5
SiglecF CF-594
cDC1
Alveolar Macrophages
Frequency (%)
Cell numbers
iii
Neutrophils
Inflammatory monocytes
NK cells
C
i
CA09
D0
D1
D4
SFB⁻ mice
0mg/kg
0.2mg/kg
0.4mg/kg
0.8mg/kg
4'-FIU, oral, daily
Determine virus titer
Harvest lungs
FACs immune cells
ii
Log 10 TCID 50/g lung tissue
CA09
0.2mg/kg
0.4mg/kg
0.8mg/kg
CA09+4'-FIU
iii
4'-FIU
48.8%
9.30%
9.21%
14.1%
8.99%
57.0%
15.3%
20.9%
21.5%
18.7%
SiglecF PE-CF594
iv
Naive
CA09
CA09+4'FIU 0.2mg/kg
CA09+4'FIU 0.4mg/kg
CA09+4'FIU 0.8mg/kg

Figure 4

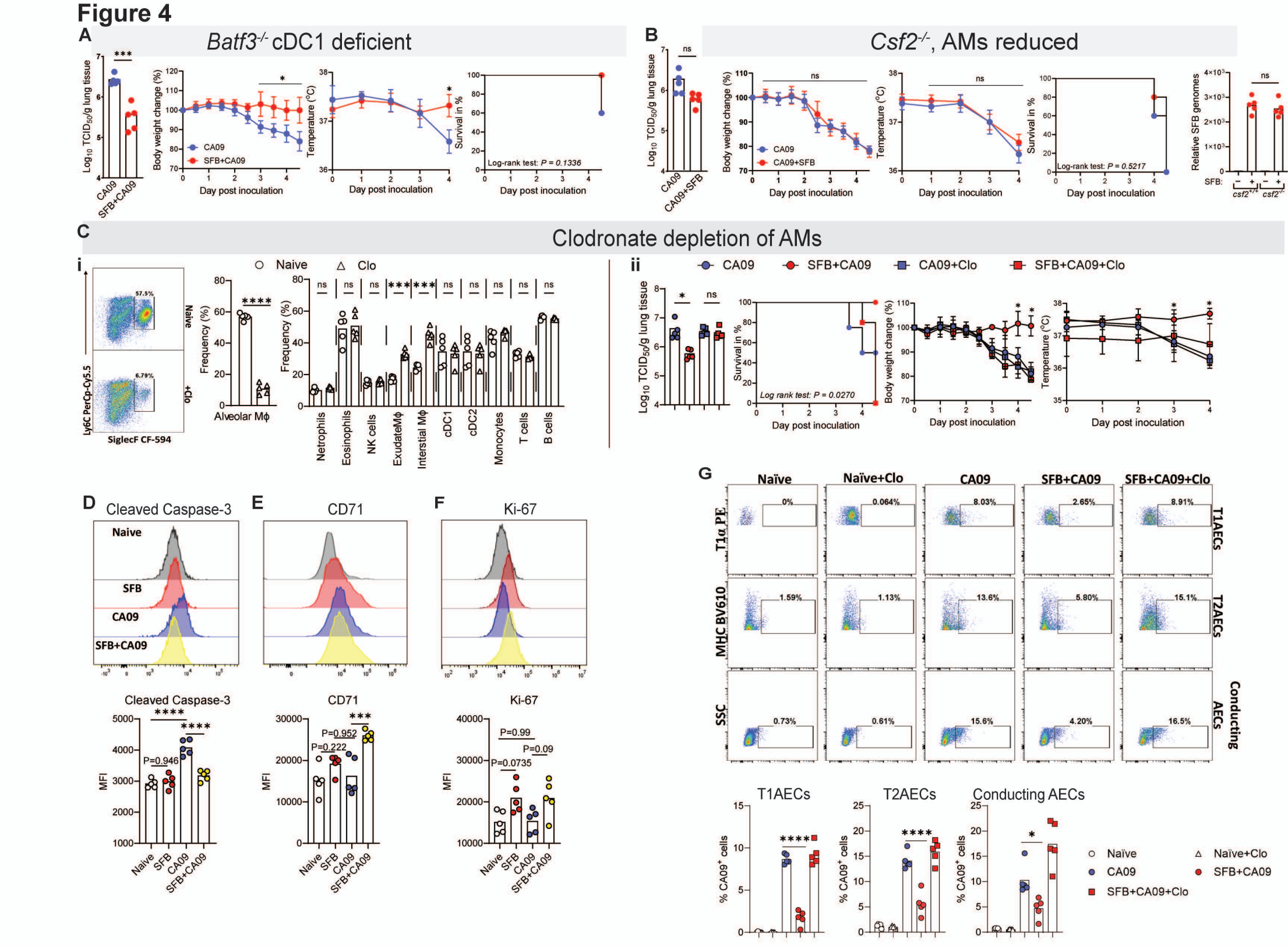
A
Batf3-/- cDC1 deficient
Log10 TCID50/g lung tissue
CA09
SFB+CA09
Body weight change (%)
Day post inoculation
Temperature (°C)
Survival in %
Log-rank test: P = 0.1336
B
Csf2-/-, AMs reduced
CA09+SFB
Log-rank test: P = 0.5217
Relative SFB genomes
SFB:
csf2+/+
csf2-/-
C
Clodronate depletion of AMs
i
Naive
Clo
Ly6C PerCp-Cy5.5
SiglecF CF-594
57.5%
6.79%
Frequency (%)
Alveolar Mϕ
Netrophils
Eosinophils
NK cells
ExudateMϕ
Interstial Mϕ
cDC1
cDC2
Monocytes
T cells
B cells
ii
CA09
SFB+CA09
CA09+Clo
SFB+CA09+Clo
Log rank test: P = 0.0270
D
Cleaved Caspase-3
E
CD71
F
Ki-67
MFI
P=0.946
P=0.952
P=0.222
P=0.0735
P=0.99
P=0.09
G
Naïve
Naïve+Clo
CA09
SFB+CA09
SFB+CA09+Clo
T1α PE
MHC BV610
SSC
T1AECs
T2AECs
Conducting AECs
0%
0.064%
8.03%
2.65%
8.91%
1.59%
1.13%
13.6%
5.80%
15.1%
0.73%
0.61%
15.6%
4.20%
16.5%
% CA09+ cells

Figure 5

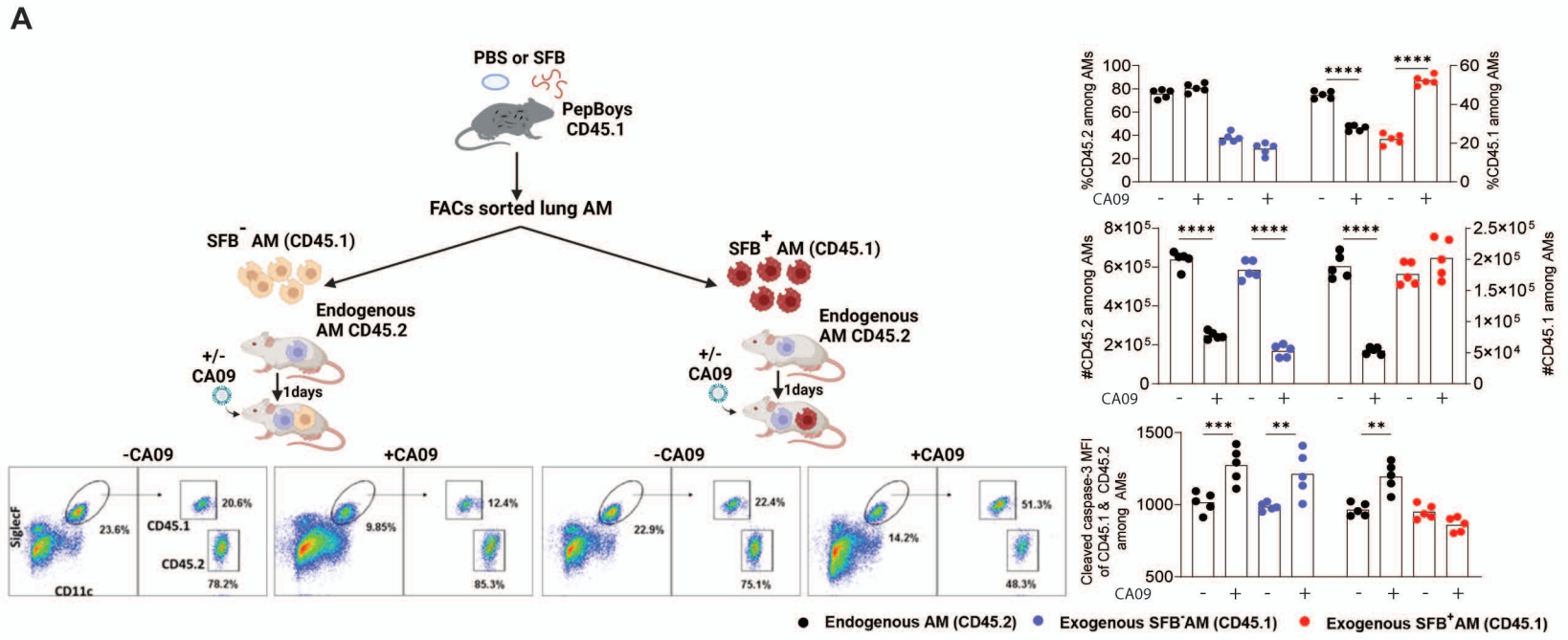
A
PBS or SFB
PepBoys CD45.1
FACs sorted lung AM
SFB- AM (CD45.1)
SFB+ AM (CD45.1)
Endogenous AM CD45.2
+/- CA09
1days
-CA09
+CA09
SiglecF
CD11c
CD45.1
CD45.2
23.6%
20.6%
78.2%
9.85%
12.4%
85.3%
22.9%
22.4%
75.1%
14.2%
51.3%
48.3%
%CD45.2 among AMs
%CD45.1 among AMs
#CD45.2 among AMs
#CD45.1 among AMs
Cleaved caspase-3 MFI of CD45.1 & CD45.2 among AMs
CA09
Endogenous AM (CD45.2)
Exogenous SFB-AM (CD45.1)
Exogenous SFB+AM (CD45.1)

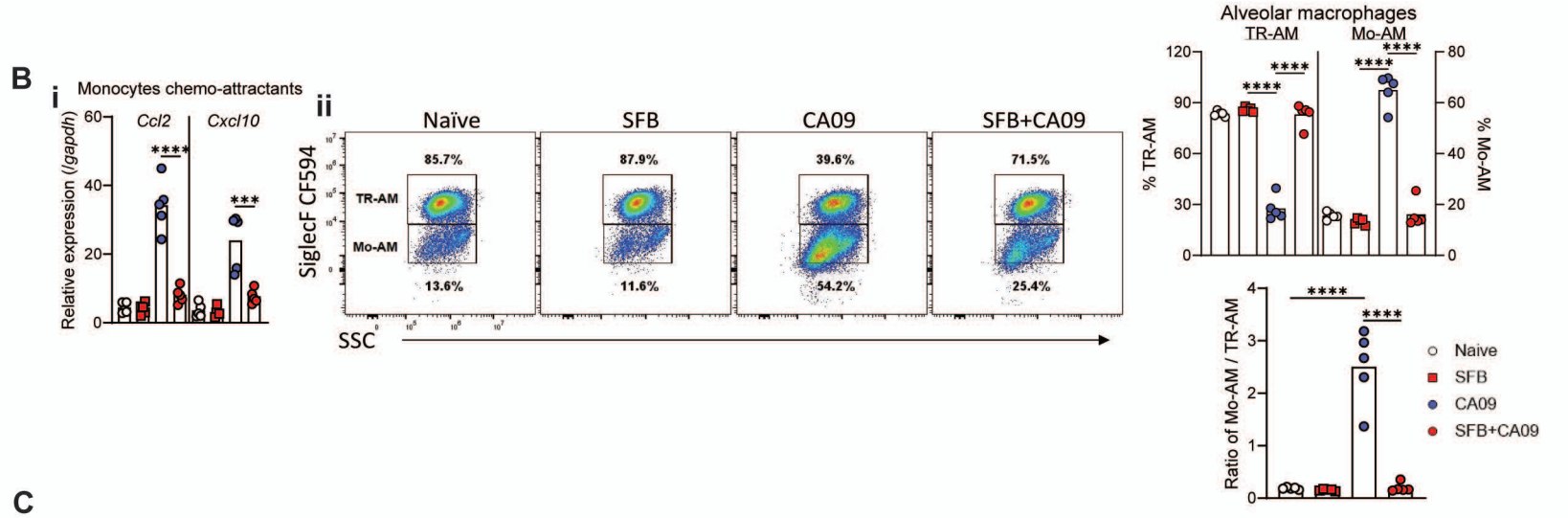
B
i
Monocytes chemo-attractants
Ccl2
Cxcl10
Relative expression (/gapdh)
ii
Naïve
SFB
CA09
SFB+CA09
SiglecF CF594
SSC
TR-AM
Mo-AM
85.7%
13.6%
87.9%
11.6%
39.6%
54.2%
71.5%
25.4%
Alveolar macrophages
% TR-AM
% Mo-AM
Ratio of Mo-AM / TR-AM
Naive
SFB
CA09
SFB+CA09

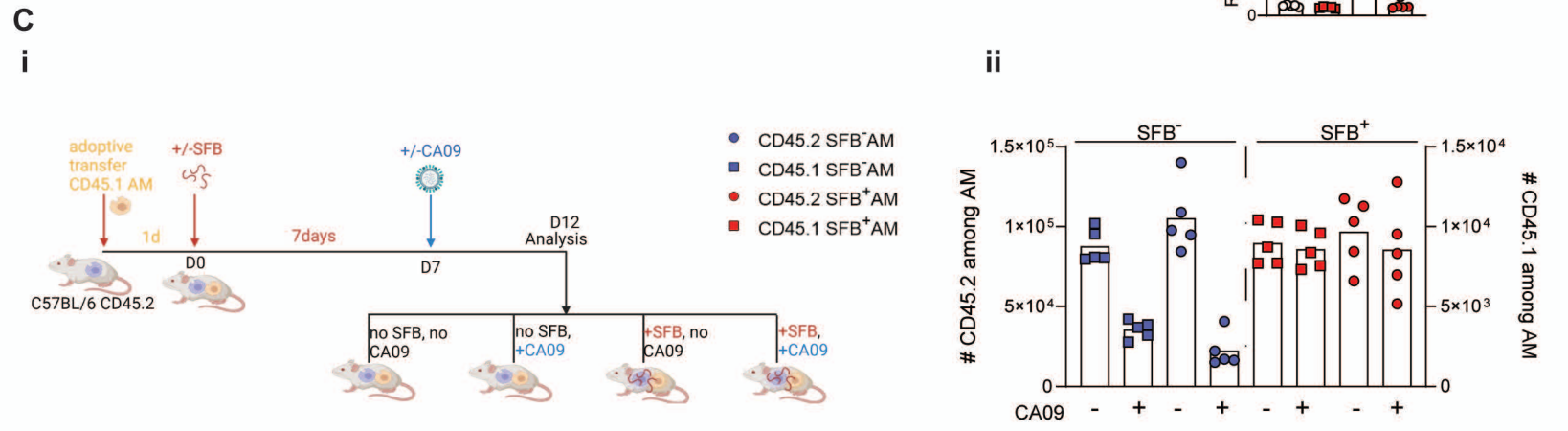
C
i
adoptive transfer CD45.1 AM
+/-SFB
+/-CA09
1d
7days
D0
D7
D12 Analysis
C57BL/6 CD45.2
no SFB, no CA09
no SFB, +CA09
+SFB, no CA09
+SFB, +CA09
CD45.2 SFB-AM
CD45.1 SFB-AM
CD45.2 SFB+AM
CD45.1 SFB+AM
ii
SFB-
SFB+
CD45.2 among AM
CD45.1 among AM
CA09

Figure 6

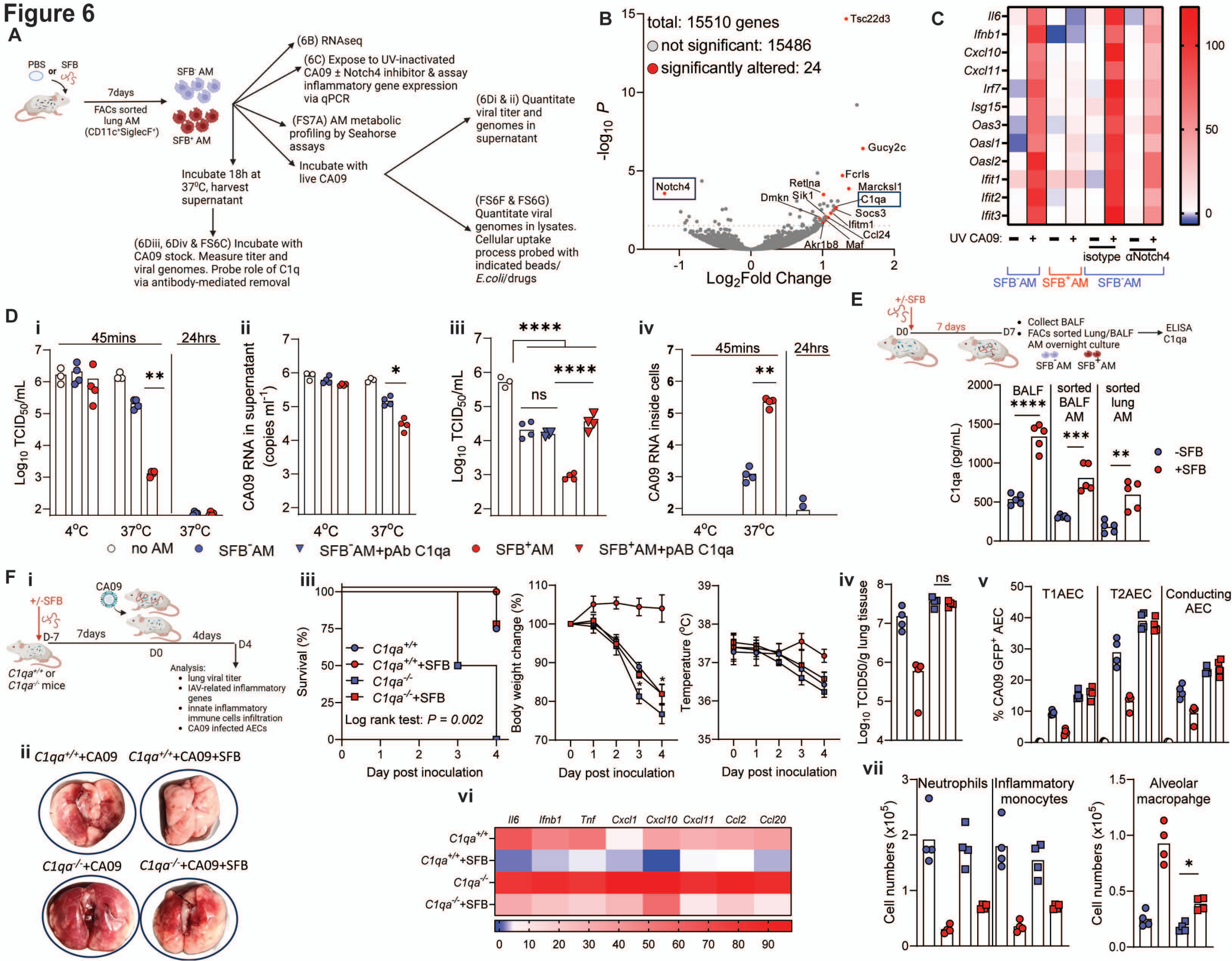
A
PBS or SFB
7days
FACs sorted lung AM (CD11c+SiglecF+)
SFB- AM
SFB+ AM
(6B) RNAseq
(6C) Expose to UV-inactivated CA09 ± Notch4 inhibitor & assay inflammatory gene expression via qPCR
(FS7A) AM metabolic profiling by Seahorse assays
Incubate with live CA09
Incubate 18h at 37°C, harvest supernatant
(6Di & ii) Quantitate viral titer and genomes in supernatant
(FS6F & FS6G) Quantitate viral genomes in lysates. Cellular uptake process probed with indicated beads/ E.coli/drugs
(6Diii, 6Div & FS6C) Incubate with CA09 stock. Measure titer and viral genomes. Probe role of C1q via antibody-mediated removal
B
total: 15510 genes
not significant: 15486
significantly altered: 24
Tsc22d3
Gucy2c
Fcrls
Marcksl1
C1qa
Retlna
Dmkn
Sik1
Socs3
Ifitm1
Ccl24
Akr1b8
Maf
Notch4
-log10 P
Log2Fold Change
C
Il6
Ifnb1
Cxcl10
Cxcl11
Irf7
Isg15
Oas3
Oasl1
Oasl2
Ifit1
Ifit2
Ifit3
UV CA09:
isotype
αNotch4
SFB-AM
SFB+AM
SFB-AM
D
i
45mins
24hrs
Log10 TCID50/mL
4°C
37°C
37°C
ii
CA09 RNA in supernatant (copies ml-1)
4°C
37°C
iii
Log10 TCID50/mL
ns
iv
CA09 RNA inside cells
4°C
37°C
no AM
SFB-AM
SFB-AM+pAb C1qa
SFB+AM
SFB+AM+pAB C1qa
E
+/-SFB
D0
7 days
D7
Collect BALF
FACs sorted Lung/BALF AM overnight culture
ELISA C1qa
SFB-AM
SFB+AM
BALF
sorted BALF AM
sorted lung AM
C1qa (pg/mL)
-SFB
+SFB
F
i
+/-SFB
D-7
7days
CA09
4days
D0
D4
C1qa+/+ or C1qa-/- mice
Analysis:
lung viral titer
IAV-related inflammatory genes
innate inflammatory immune cells infiltration
CA09 infected AECs
ii
C1qa+/++CA09
C1qa+/++CA09+SFB
C1qa-/-+CA09
C1qa-/-+CA09+SFB
iii
Survival (%)
C1qa+/+
C1qa+/++SFB
C1qa-/-
C1qa-/-+SFB
Log rank test: P = 0.002
Day post inoculation
Body weight change (%)
Day post inoculation
Temperature (°C)
Day post inoculation
iv
Log10 TCID50/g lung tissue
ns
v
T1AEC
T2AEC
Conducting AEC
% CA09 GFP+ AEC
vi
Il6
Ifnb1
Tnf
Cxcl1
Cxcl10
Cxcl11
Ccl2
Ccl20
C1qa+/+
C1qa+/++SFB
C1qa-/-
C1qa-/-+SFB
vii
Neutrophils
Inflammatory monocytes
Alveolar macropahge
Cell numbers (x10^5)

Figure 7

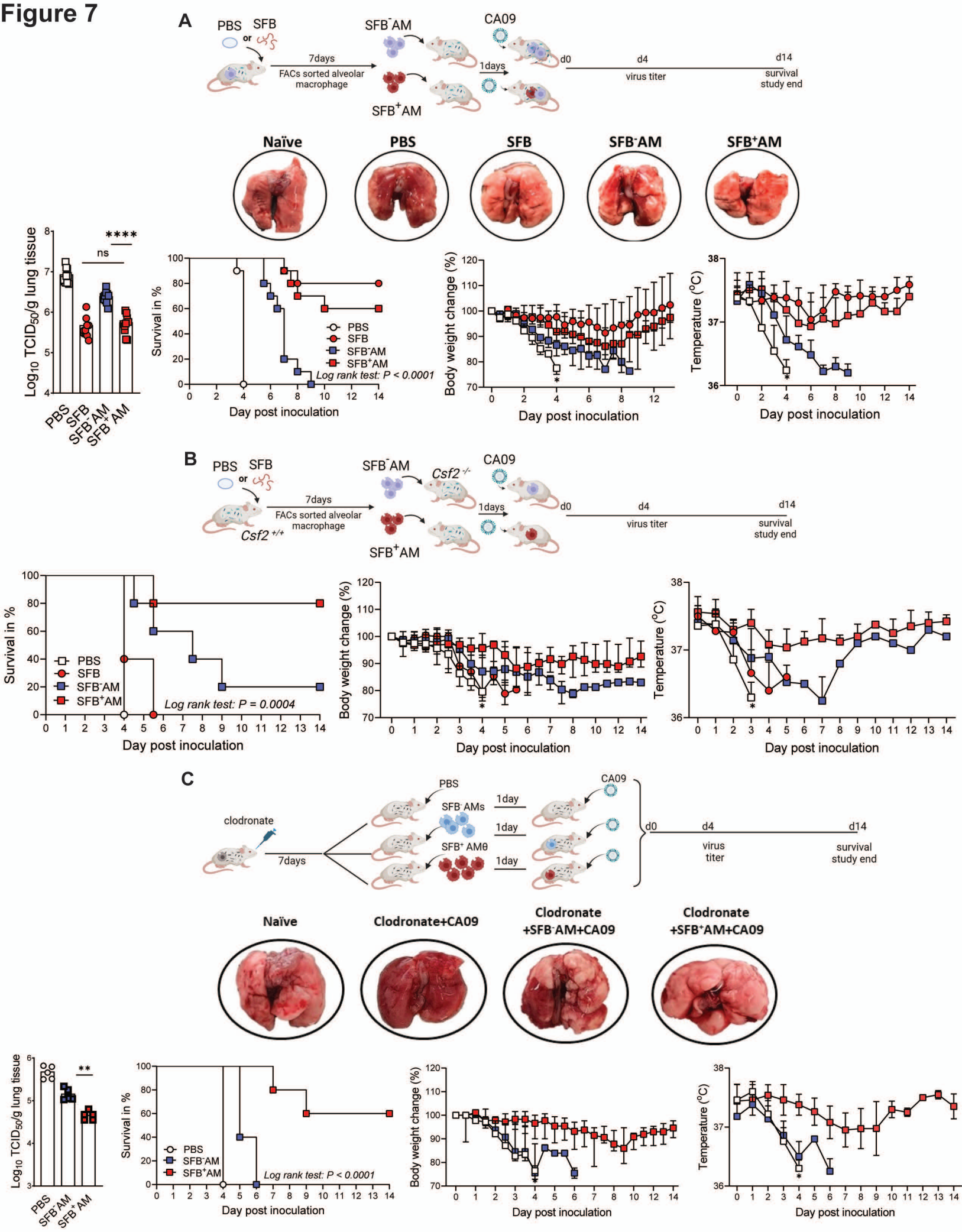
A
PBS
SFB
or
7days
FACs sorted alveolar macrophage
SFB⁻AM
SFB⁺AM
CA09
1days
d0
d4
virus titer
d14
survival study end
Naïve
PBS
SFB
SFB⁻AM
SFB⁺AM
Log10 TCID50/g lung tissue
****
ns
Survival in %
Log rank test: P < 0.0001
Day post inoculation
Body weight change (%)
Temperature (°C)
B
Csf2 -/-
Csf2 +/+
Log rank test: P = 0.0004
C
clodronate
PBS
SFB⁻AMs
SFB⁺ AMθ
1day
Naïve
Clodronate+CA09
Clodronate +SFB⁻AM+CA09
Clodronate +SFB⁺AM+CA09
**

Figure S1 (related to F1)

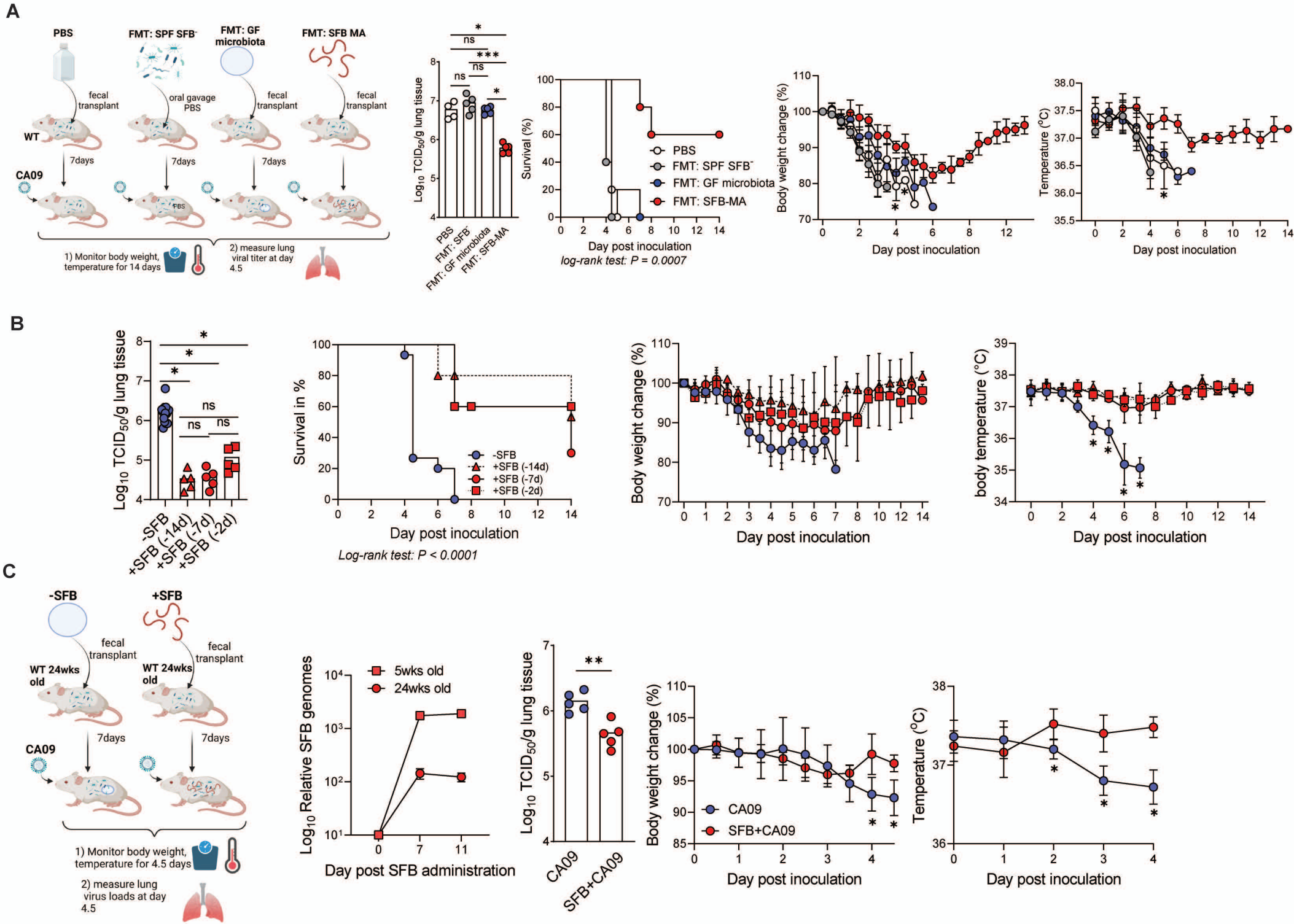

Figure S2 (related to F3)

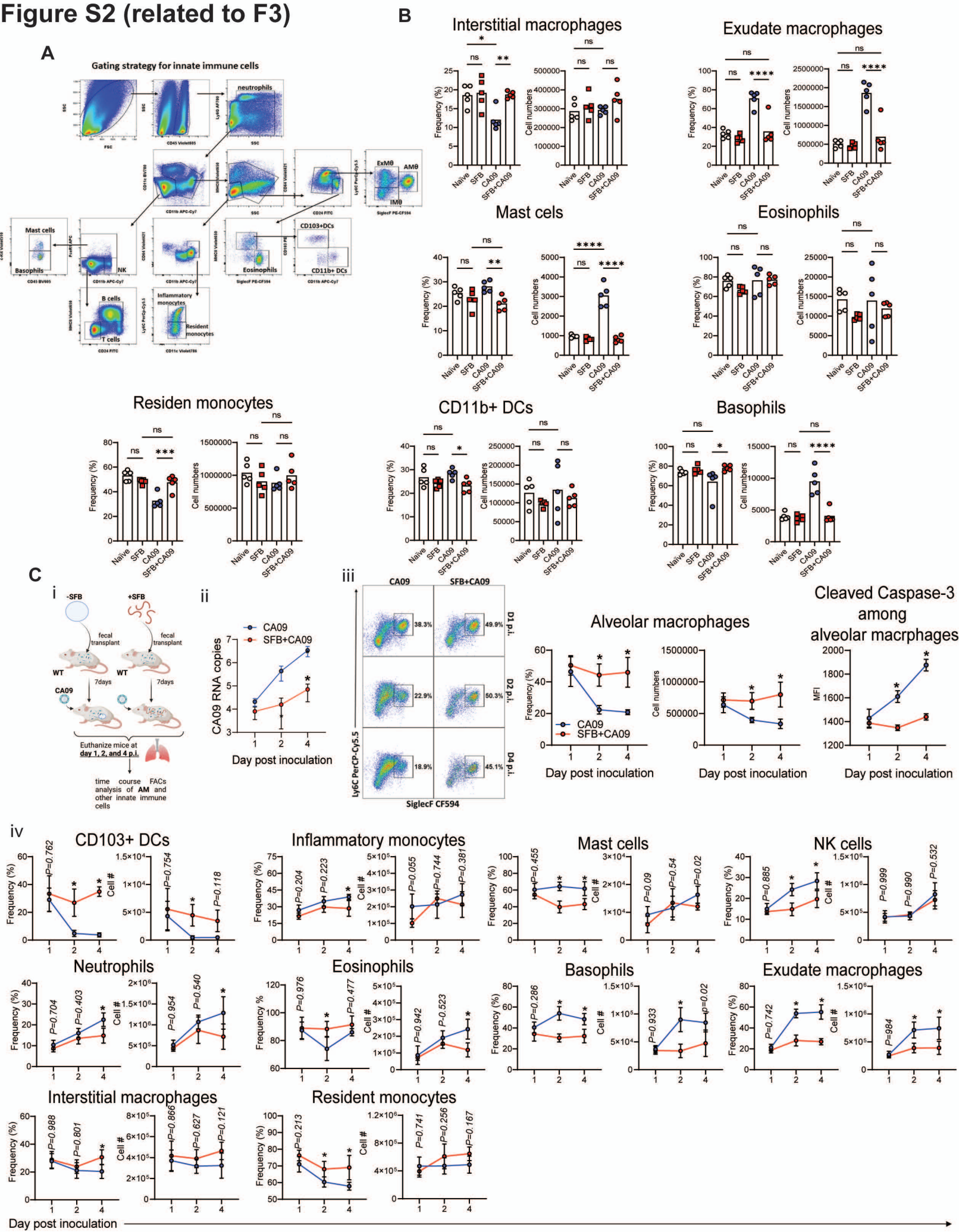

Figure S3 (related to F4)

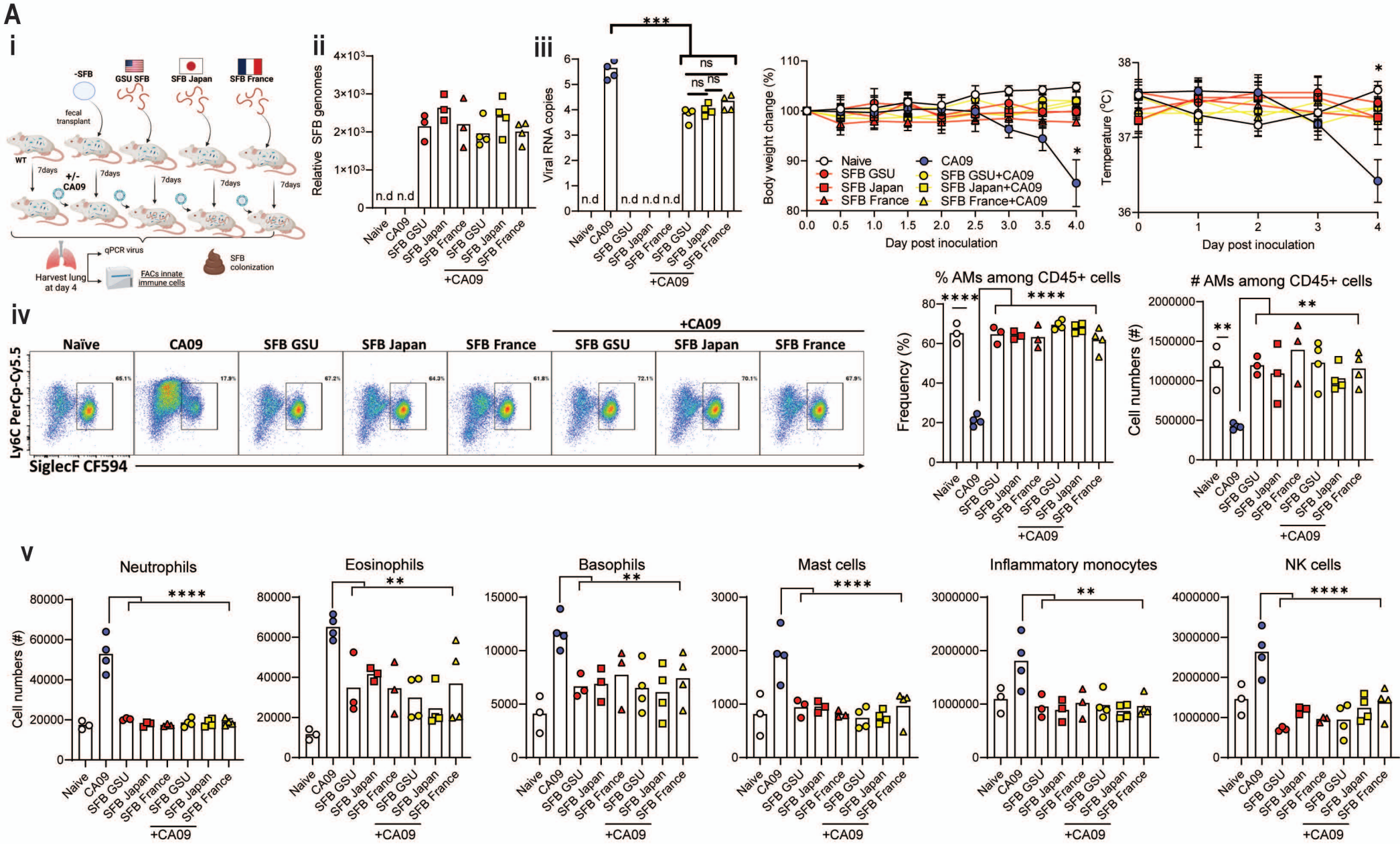

Figure S4 (related to F4)

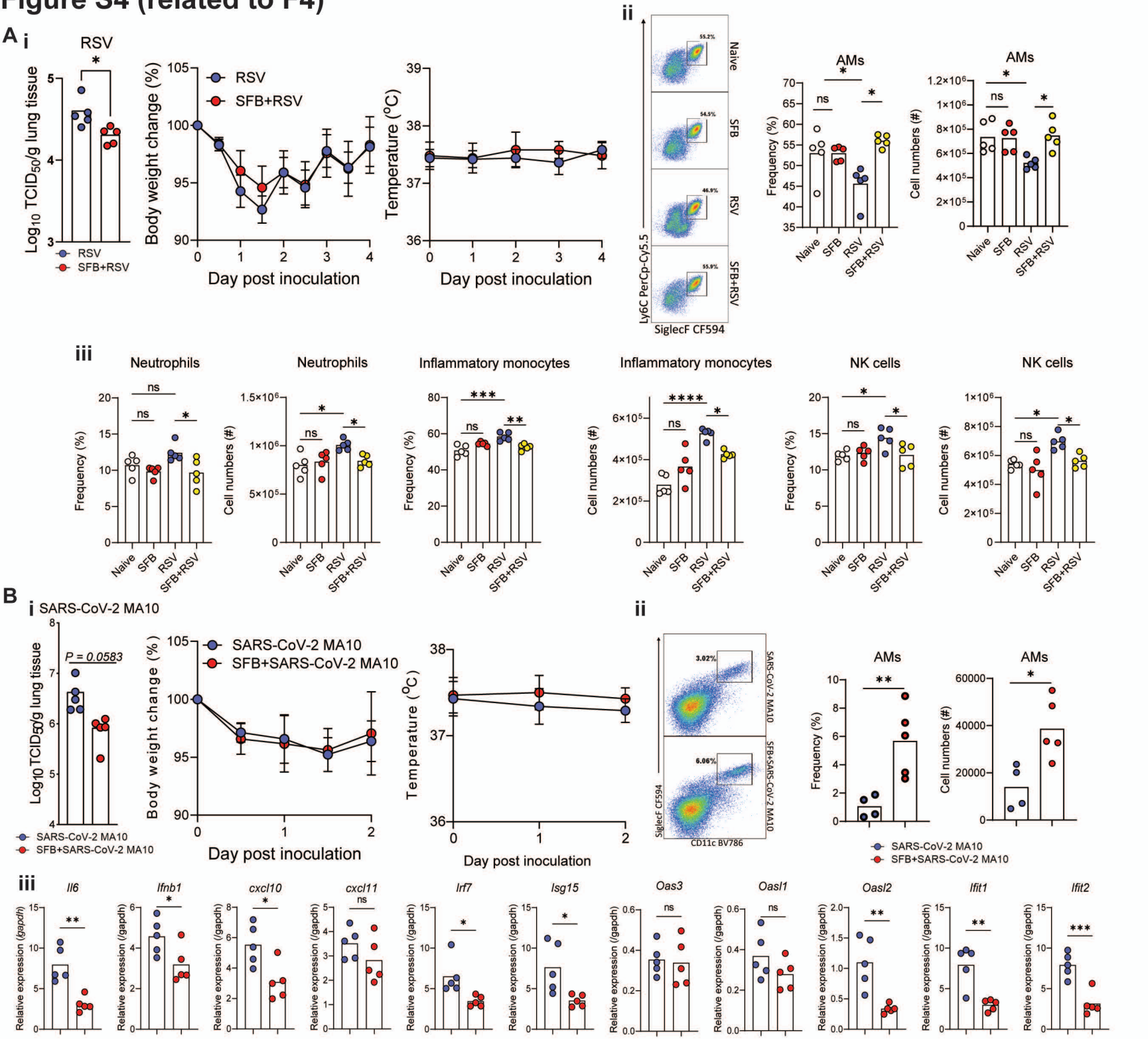

Figure S5 (related to F4)

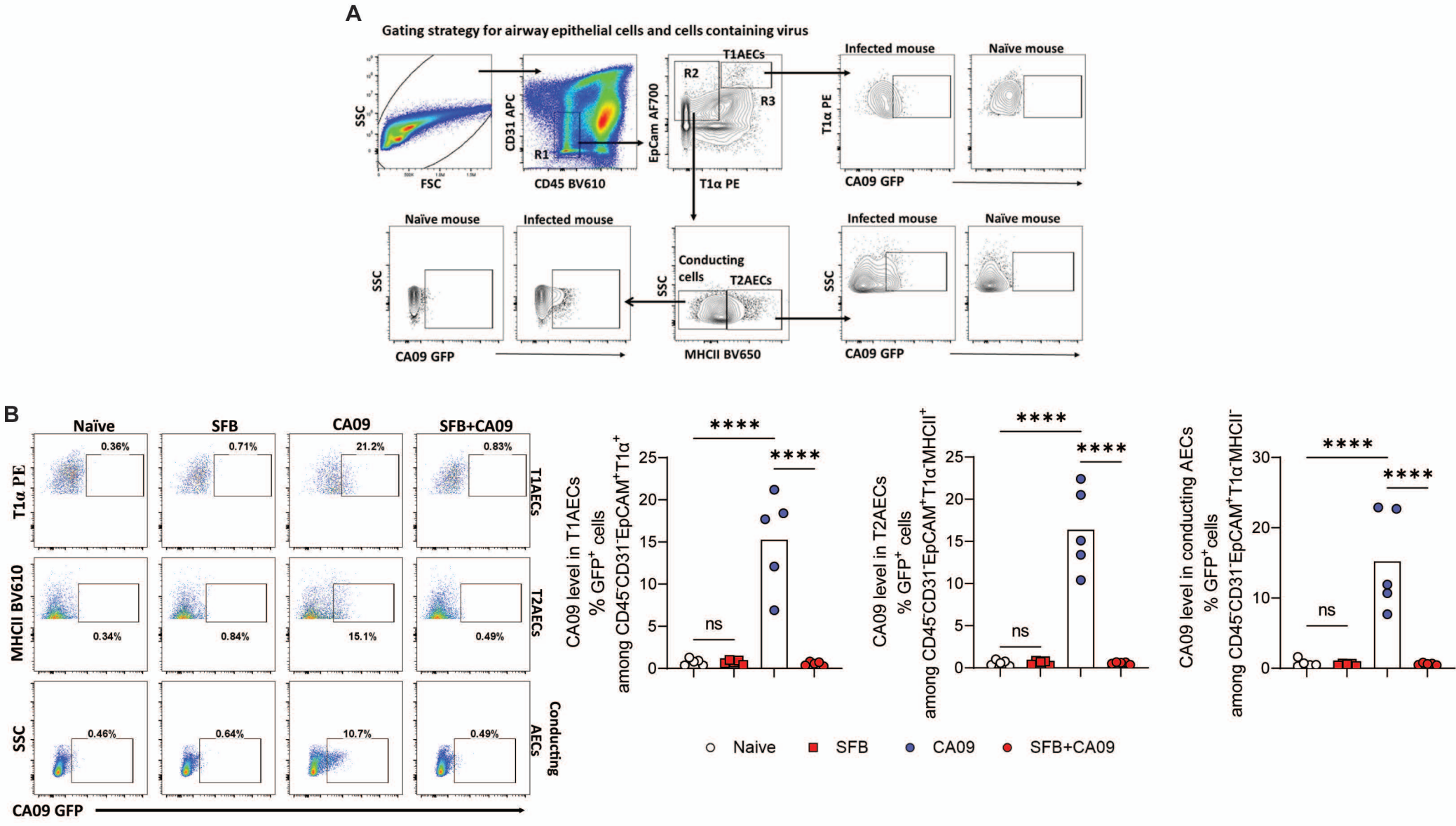

Figure S6 (related to Fig 6)

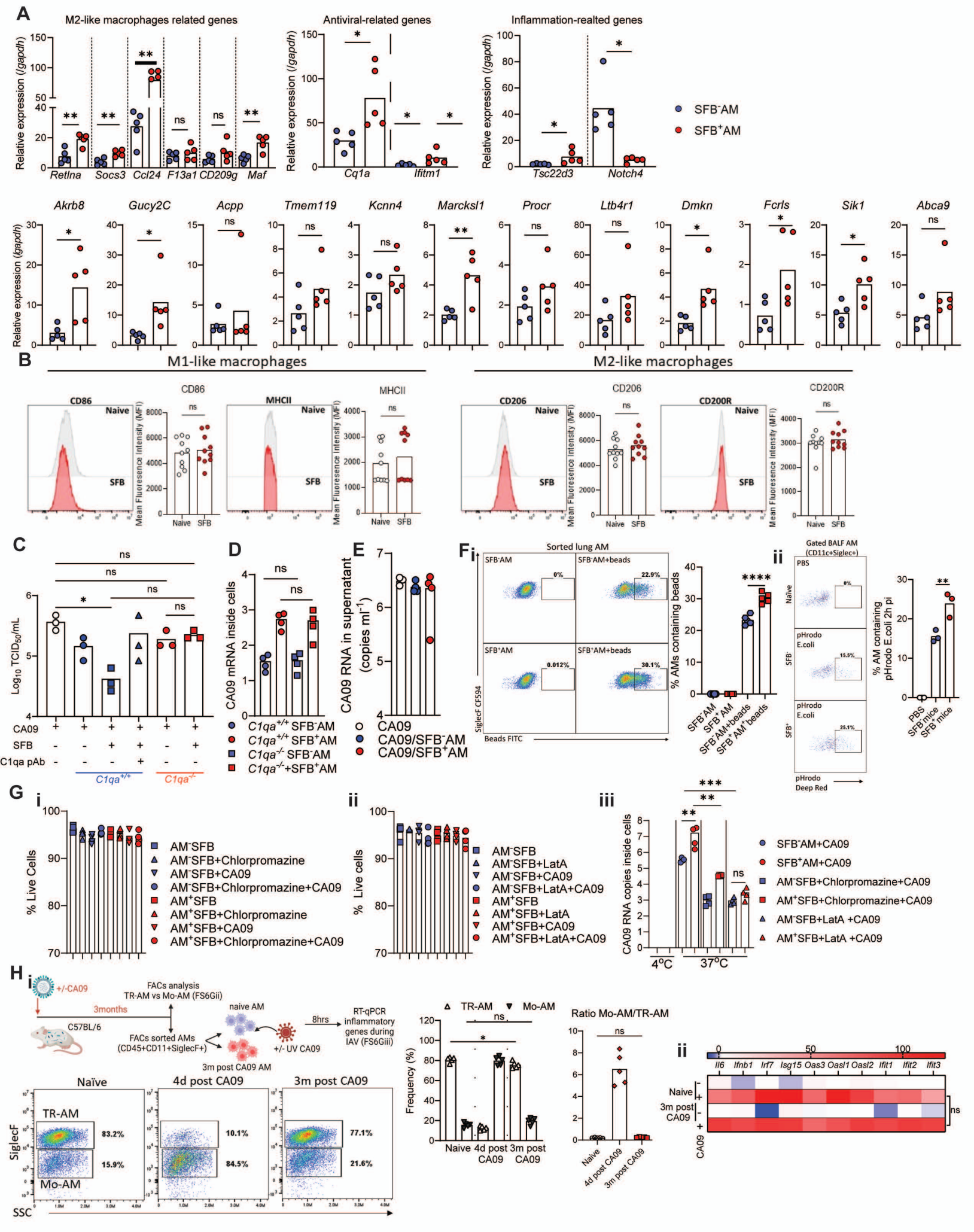
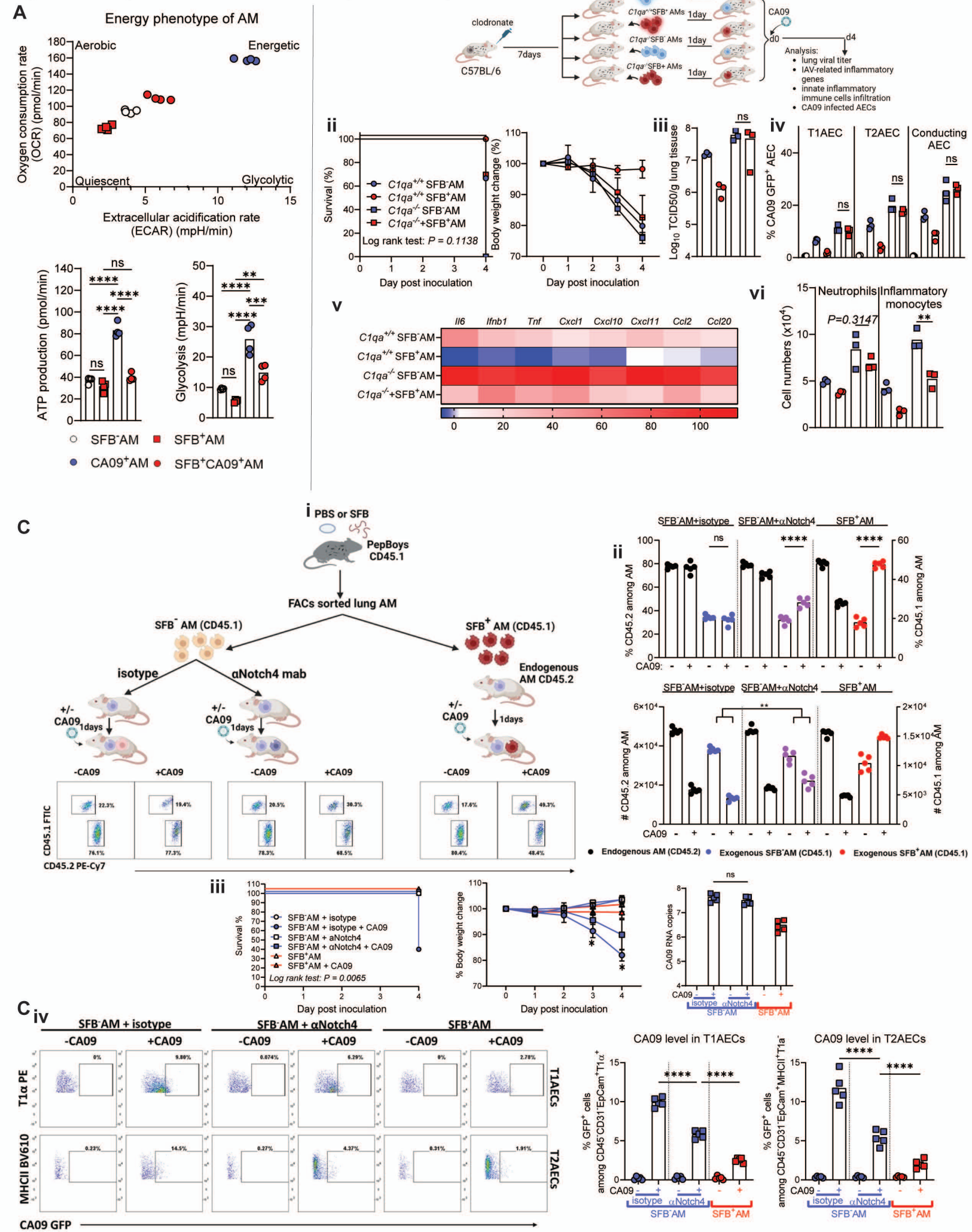
Figure S7 (related to F6 & F7)